Topology, kinetics and inheritance in clonal colonies of bone marrow stromal cells

Alessandro Allegrezza[1], Riccardo Beschi[1], Domenico Caudo[1,2] Andrea Cavagna[3,1,4,*], Alessandro Corsi[5], Antonio Culla[3], Samantha Donsante[5,¤a] Giuseppe Giannicola[6], Irene Giardina[1,3,4], Giorgio Gosti[2,¤b] Tomas S. Grigera[7,8,9,3], Stefania Melillo[3,1], Biagio Palmisano[5,3], Leonardo Parisi[3,1], Lorena Postiglione[3,¤c], Mara Riminucci[5], Francesco Saverio Rotondi[1]

1 Physics Department, Sapienza University, Rome, Italy
2 Center for Life Nano & Neuro Science, Italian Institute of Technology, Rome, Italy
3 Institute for Complex Systems, National Research Council, Rome, Italy
4 Istituto Nazionale di Fisica Nucleare, Sezione Roma 1, Rome, Italy
5 Department of Molecular Medicine, Sapienza University, Rome, Italy
6 Department of Anatomical, Histological, Medico Legal and Orthopaedic Sciences, Sapienza University, Rome, Italy.
7 Instituto de Física de Líquidos y Sistemas Biológicos CONICET - Universidad Nacional de La Plata, La Plata, Argentina
8 CCT CONICET La Plata, Consejo Nacional de Investigaciones Científicas y Técnicas, Argentina
9 Departamento de Física, Facultad de Ciencias Exactas, Universidad Nacional de La Plata, Argentina

¤a Current Address: Tettamanti Center, Fondazione IRCCS San Gerardo dei Tintori, Monza, Italy

¤b Current Address: Institute of Heritage Science, National Research Council, Rome, Italy

¤c Current Address: Dipartimento di Ingegneria Chimica, dei Materiali e della Produzione Industriale, Università degli Studi di Napoli Federico II, Napoli, Italy

* andrea.cavagna@roma1.infn.it

Abstract

Bone marrow stromal cells (BMSCs), whose populations contain multipotent skeletal stem cells with relevant therapeutic applications, are known to produce very heterogeneous colonies upon *in vitro* culture, a trait that may severely hinder the clinical usefulness of BMSC-based therapies. Therefore, reaching a better insight on the nature of such heterogeneity, as well as on the factors determining it, is important. Here, by using time-lapse microscopy, we study the structure of $N = 28$ human BMSC colonies from six donors, each colony derived from a single cell, and trace their lineage trees up to the seventh generation. We confirm the presence of very significant inter-colony and intra-colony heterogeneities, both in the topology of the lineages and in the replicative kinetics of the colonies. We also find that topology and kinetics are strongly correlated, consistent with the existence of regulating factors linking the sub-population of inactive cells, which uniquely determine a lineage's topology, and that of active cells, which are the sole responsible for the proliferation rate of the colony. Finally, we submit each colony to an entropy-based inheritance test, which measures the degree of non-random clustering of inactive cells within the same branches of the lineage, and find a clear signature of hereditary transmission of the probability of emergence of inactive cells in the largest majority of the experimental lineages.

Author summary

The topological structure of the lineage tree produced by the growth of a stem cell colony is uniquely determined by the number of its inactive cells and their position along the tree's branches. Inactive cells do not divide (be it because they are temporarily quiescent, or because they are permanently senescent or differentiated), and therefore do not contribute to the statistics of the division times of the colony, while the active portion of the population proliferates with a kinetics that characterises the colony's growth as a whole. Being these two phenotypes (active vs inactive) well-separated from each other, there are no *a priori* reasons to expect a specific connection between the structure of the inactive part of the population and the replicative speed of the active part. However, we do find strong evidence of such connection in BMSCs: colonies with many inactive cells are also characterized by a slow growth of their active cells population, and *vice versa*. Interestingly, our experimental results cannot be explained by random fluctuations in the lineage structure, as an entropy-based inheritance test indicates that the probability of emergence of inactive cells has a strong hereditary character.

Introduction

Bone marrow stromal cells (BMSCs) are adherent, fibroblast-like cells that are isolated from the post-natal bone marrow and are able to generate skeletal tissues and establish a functional bone marrow microenvironment upon *in vivo* heterotopic transplantation [1]. BMSCs contain a small subset of cells that are able to proliferate even in low density cultures – i.e. in the absence of paracrine stimuli produced by neighbouring cells – to form colonies [1, 2]. These BMSCs, competent for density-insensitive growth, include skeletal stem cells (SSCs) and progenitor cells normally residing in the post-natal bone marrow [3–5]. Therefore, they are the repository of the regenerative properties observed in *in vivo* assays and are critical to any potential therapeutic application of BMSCs.

Colony-forming BMSCs share many biological features, including the expression of specific surface markers that can be used for prospective purification [6–8]. However, the colonies that they generate are heterogeneous in nature and show considerably different *in vivo* behaviour. Indeed, colonies formed by BMSCs corresponding to genuine SSCs undergo multilineage differentiation and organise a bone marrow microenvironment, whereas colonies derived from BMSCs corresponding to more committed progenitor cells produce only bone [4, 9]. Furthermore, some colony-forming BMSCs generate a progeny that maintains the fibroblast-like phenotype and does not perform any specific function [4].

The heterogeneous and unpredictable *in vivo* behaviour of BMSC colonies is one of the most important factors preventing the development of standard, large-scale therapeutic approaches for skeletal tissue regeneration. For this reason, several studies have attempted to identify morphological and/or molecular features expressed *in vitro* that correlate with the differentiation properties displayed *in vivo* [9–11]. However, although interesting data on BMSC biology have emerged, no predictive parameters have been identified as yet, so that heterotopic transplantation remains the only approach to unambiguously identify the *in vivo* fate of BMSC colonies. Therefore, new methods to prospectively sort out BMSC colonies with similar potency need to be explored.

Lineage studies are a promising approach in this respect. First, by carefully tracing the proliferation of colonies derived from different single cells and by studying their developmental differences, we can try to identify the origin of the initial variability among initiator cells, which leads to the subsequent *inter-colony* heterogeneity that we wish to control. In this context, it is of particular interest whether the variability among initiator cells belonging to the same donor and expanded within the same experiment in the same exact conditions is any different from the variability across different experiments and even different donors (as we shall see, this is not the case). Secondly, different parts (or branches) of the same colony may develop rather differently in terms of proliferation rate, number of inactive cells, etc., a phenomenon called *intra-colony* heterogeneity; in these cases, it is reasonable to assume that this difference emerged at some point during proliferation stemming from the originating cell. Following as accurately as possible the early stages of this proliferation seems therefore a potential way to sort out how – and at what point in the lineage – such differences arise.

Time-lapse microscopy has been used extensively to reconstruct the lineage of both embryonal and adult cell colonies [12–17]. In the case of BMSCs [18–21], the technical challenges are considerable, starting from the image tracking of the individual cells, so that lineage studies often follow proliferation for the first few generations (typically five). Irrespective of the technical differences, all studies have highlighted a great heterogeneity in many different parameters characterising both the individual cell morphologies and the collective properties of the BMSC colonies; moreover, it has

been explicitly proved that colonies may have significant variability in their differentiating potential [18, 20]. Another crucial aspect highlighted by some studies [8] is that when we are unaware of the lineage we may be lured into thinking that one fully developed colony that is well separated from other colonies in the plate, must have been originated from one single cell, while this is very emphatically not true: even when plated at very low densities, BMSCs tend to cluster, hence one can have very early merging of different colonies into single collective units, merging that becomes completely undetectable later on in the proliferation. Clearly, when this happens not only the role of heterogeneities is even stronger, but it is also sneakier, in that it dangerously confounds inter-colony with intra-colony heterogeneity. This is yet another reason why the study of 'clonal' colonies should only be performed through full lineage tracing and in particular why single-cell derived colonies are so important in this type of study. Focusing a lineage study on single-cell derived colonies is, however, technically difficult and very time-consuming, hence no lineage studies to date presents a number of single-cell derived colonies larger than 10, which is borderline for statistical analysis.

Here, we conduct a study of BMSCs proliferation *in vitro* through time-lapse microscopy, reconstructing the full lineage of 28 single-cell derived colonies up to the seventh generation. By seeding the plate at very low densities, we are able to only select colonies that derive from single, well-isolated cells and that never get in contact with each other, so that we are certain of the clonal nature of each colony. We characterise colonies according to two major traits: the topology of their lineage – namely how many leaves and how many inactive cells their trees have – and the kinetics of the colony – as expressed by the statistics of the division times of the cells and by the proliferation rate of the colony. We show that, although both these traits are strongly heterogeneous, fluctuations in topology and kinetics are not independent from each other, unveiling a strong correlation between the two, a correlation that connects the propensity of the colony to produce inactive cells (typically G_0 cells) to the proliferation properties of the sub-population of active cells.

The existence of a correlation between topology and kinetics at the collective level of the entire colony indicates that the cell-to-cell variability cannot be completely random, otherwise it would wash out the overall character of the entire clonal colony as a single unit. Indeed, a lineage at generation seven may contain up to $2^7 = 128$ cells: with such a large number, if cells' parameters fluctuated independently from cell to cell, short and long division times within the colony would compensate each other and we would not observe any collective correlation. This suggests that a certain degree of inheritance is at work in BMSCs colonies, even at the level of the simple observables we consider here. Hence, our next focus will be to quantify the strength of inheritance, and we shall indeed find that the large majority of BMSC colonies in the study have a structure that can only be explained by a clear hereditary transmission of the probability to become inactive.

Results and Discussion

Description of the data

Detailed methods are located following the Conclusions, for better manuscript readability; here we present a brief summary of the experimental protocol. Data were collected during the course of 9 experiments, from January 2023 to March 2025. Human bone marrow stromal cells were isolated from bone samples harvested from 6 different healthy donors undergoing elbow orthopaedic surgery, and were plated at passage P0, P1, or P2, depending on the experiment (see Table S1 for details).

BMSCs were seeded in 35mm culture dish at very low density (10-20 cells/dish), in order to produce colonies derived only from single, spatially isolated cells. The growth of the colonies was studied up to generation $k = 7$, with phase contrast time-lapse microscopy, recording high resolution images at 20X, every 15-20 minutes, depending on the experiment (Table S1). To ensure unequivocal identification of cells and mitosis, the tracking of individual cells was performed manually via a custom semi-automatic software developed on purpose; no unsupervised algorithm has been used. If colonies get in contact with each other during the time-lapse, or if one or more cells drop out of the field of view, we discard the colonies. A motorised translational stage is used to monitor several colonies in parallel within the same dish; typically, each experiment produced 3-4 viable colonies (Table S1), and we obtained in total 28 single-cell derived BMSC colonies. As we shall see, colonies kinetics' strongly fluctuates, a trait that influenced the variability of the experiments' duration: a single experiment could last between 10 to 14 days; the time at which a colony reaches the seventh generation can be as short as 5 days for fast colonies and significantly larger than that for slower colonies. We note that, in contrast with most time-lapse experiments on BMSCs and other cell types, we do not fix the total time of the experiment, but we fix the maximum generation ($k = 7$), keeping the experiment going until all active cells in a colony have arrived to $k = 7$. The reason is that keeping the total observation time fixed may introduce a bias both in the statistics of the division times and in the reconstruction of the lineage tree [22], which are the main features that we wish to investigate; even though this choice requires substantial additional experimental and tracking effort, it is crucial to our analysis. In Fig.1 we present sample images of the time lapse following the growth of one of the colonies in the dataset, from the single cell scale, up to the scale of the entire dish.

The maximum number of cells at the seventh generation is $2^7 = 128$, but not all cells keep dividing, hence the total number of cells of the colonies has large fluctuations. We only include in the study colonies that produce *at least* two cells at generation $k = 7$, lest the seventh generation criterion of the whole study becomes void. We call *active* those cells for which we observe a mitosis and therefore record a division time. Not all cells are active; some cells stop dividing, thus entering what is normally called the G_0 phase [23–25]. In the present study we classify a cell as G_0 if it does not divide within 84 hours (3.5 days) from the moment it was born; this threshold must be compared to the mean division time of BMSCs, which is 20 hours.[1] In general, cells in the G_0 phase can be in a reversible state (quiescent) or in an irreversible state (senescent or differentiated) [24, 26]. A previous study of BMSC colonies [19] – albeit at passage P5, quite larger than the P0, P1, P2 of our study – has established through the β-galactosidase assay that most cells in the G_0 phase were senescent. Moreover, several studies [19, 27, 28] established a clear correlation between senescent state and morphology: senescent cells have typically a much larger area and are characterized by a flat morphology different from the spindle-like shape of proliferating cells. This is also the case in our data (Fig.1, bottom). Nevertheless, because in the present study we did not run the β-galactosidase assay, we prefer to use the less committed label 'G_0' for cells that stop dividing.

In very few cases cells commit apoptosis and die; apoptosis is very clear in the imaging (the cell bursts and detaches from the plate), hence no particular criterion is needed to define it. As we shall see later on, despite the obvious biological difference

[1] In only three cases we were not able for technical reasons to follow a G_0 cell up to the full 84 hrs criterion: in colony 20241112-02 one cell was tagged as G_0 after 68 hrs; in colony 20250313-14 two cells were tagged as G_0 after 57 hrs. The morphology of these cells, though, was very typical of the G_0 state. Moreover, all three cells belonged to the last full generation, $k = 6$, hence even in the unlikely case that their G_0 status changed, the topology of their trees would not be affected significantly.

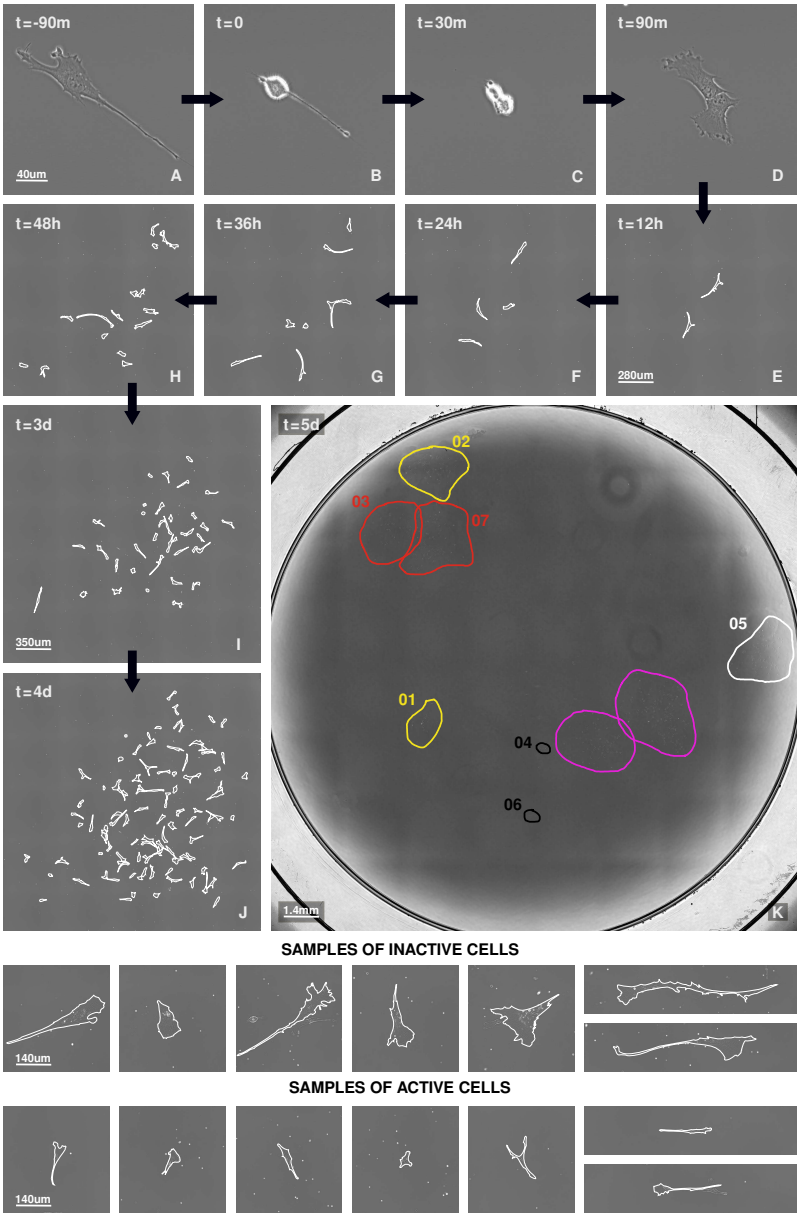

Fig 1. Time-lapse of a BMSC colony. (A-K) Images follow the evolution in time of colony 20241112-05 from its single originating cell. Panels (A-J) are different scale crops of images acquired at magnification 20X. To enhance visibility, in panels (H-J) cell contours are drawn in white. **(A)** The originating cell as it appears 90 minutes before its mitosis. **(B)** During the mitotic rounding phase (MRP), cells assume a bright and almost spherical shape, easily detectable in the images. We use the MRP as a marker for mitosis. The MRP of the originating cell marks the temporal beginning of the colony development; hence it defines a reference time start ($t = 0$) for the colony. **(C)** Half an hour after the beginning of MRP, the two daughter cells still have a spherical shape. **(D)** At $t = 90$ minutes, the two daughters distinguishable from their well-separated nuclei. **(E-H)** Within the first 48 hours, the colony expands to the fourth generation. **(I-J)** The third and the fourth day the colony expands to the fifth and sixth generation. The colony is still well isolated, with a typical cell-to-cell distance much smaller than the distance from the borders of the image and from cells belonging to other colonies. **(K)** Overview at magnification 4X of the entire dish at day five for experiment 20241112 (8×8 photo tessellation). The white contour encloses the colony described in panels (A-J). Yellow contours indicate isolated colonies, which we still follow on day five; red contours indicate infiltrated colonies (colonies that got in contact with each other), which we stop recording. Purple circles denote colonies derived from cells that we did not select at the beginning of the experiment because of their close proximity. Finally, the two small black circles correspond to cells that were selected but never got into the mitotic state, not giving rise to any colony. **Bottom strips**. Samples of G_0 and active cells at the same magnification. Cell contours were manually drawn in white to enhance visibility. G_0 cells have a different morphology, typically flat, occupying a larger area than the spindle-shaped active cells.

between G_0 and dead cells, they have the same effect on lineage topology, as they both interrupt their branch of the tree, due to their lack of progeny. It is therefore useful for the sake of the present study to assign a name to cells that are either G_0 or dead, hence we call these *inactive* cells. In this way, the total population within a colony is given by the union of its active and inactive cells, while the inactive sub-population is given by the union of G_0 and dead cells (in fact, only 17 cells die in our whole dataset, which is just the 5% of all 285 inactive cells; hence inactive cells are mostly G_0 – see Table S1).

Representation of the lineage trees

We adopt an abstract radial representation of the lineage trees (Fig.2), similar to the one used in Ref. [29, 30]: each node represents a mitosis and each link between two nodes represents a cell. Unlike in more standard representations [19, 21], the length of the link is *not* proportional to the division time of the cell (or cell cycle time); here, each link has the same standard length, so that every lineage occupies the same graphical area. Instead, we represent the value of the division time of each cell by a colour scale associated to the segment representing that cell: a light green segment corresponds to a cell with a short division time (fast cell cycle), while a dark blue segment corresponds to a long division time (slow cell cycle). Because we do not know the absolute time at which the first cell of the colony was born, there is no link representing it; on the other hand, we do know when this first cell divides, which is the first mitosis of the colony (marked by $t = 0$ in Fig.1), represented by the central node (or root) of the tree. In this kind of tree, elliptical contours separate different generations, so that mitosis of cells belonging to the same generation lie on the same ellipse, while cells belonging to the same generation are represented by segments belonging to the region between two consecutive ellipses. We trace cells up to generation $k = 7$, which means that the last divisions we observe are those between the $k = 6$ and the $k = 7$ generations; hence, we do not measure the division times of the $k = 7$ cells, which are therefore represented in grey.
In some cases the lineage is perfectly whole and round, so that all branches reach generation $k = 7$; this happens when no inactive cells emerge in the colony up to the last generation. On the other hand, in most of the colonies inactive cells (mostly G_0) do emerge during proliferation. An inactive cell terminates the proliferation of the tree along that particular branch, hence there is no node/mitosis at the end of an inactive link/cell; because an inactive cell does not divide, it does not have a division time and we conventionally paint it black. We represent an inactive-G_0 cell by a short black cap at the end of the link and an inactive-dead cell with a red circle at the end of the link (Fig.2). We stress that this abstract representation of the lineage contains no information what-so-ever about the actual positions, and mutual distances, of the cells in the physical space of the dish. Cells move a lot during the development of the colony, in particular during the early stages, and this dynamics in physical space is not present in the lineage tree, which only contains the genealogical relations between the cells. Although some degree of correlation exists between distance on the tree and distance in physical space, this correlation is not very stringent (Spearman correlation coefficient $\rho = 0.24$ – see Fig.S2); hence, it is important not to assume that proximity in physical space implies proximity in the lineage tree.

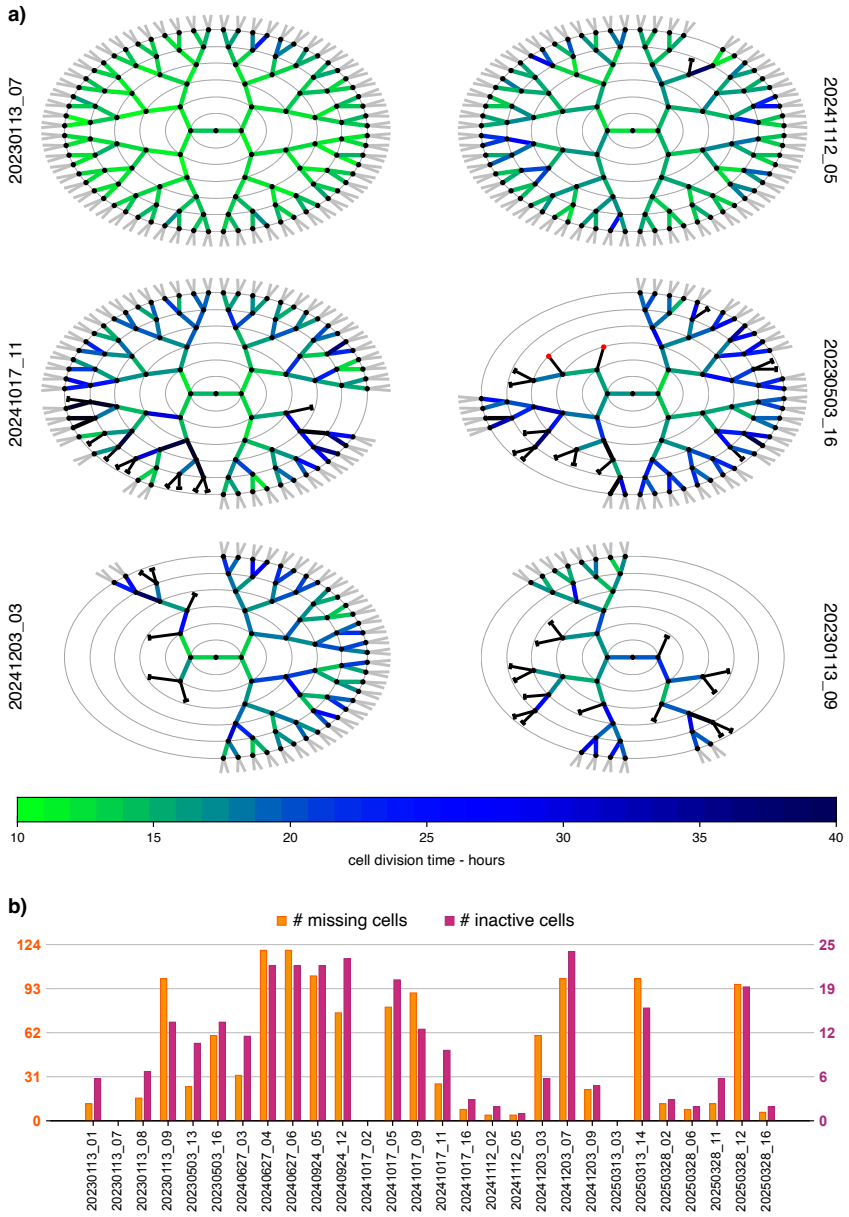

Fig 2. Topology – Lineage trees. a) Abstract representation of the lineages of six BMSC colonies in the dataset. Each node (black dots) represents a mitosis and each link between two nodes represents a cell; the central node is the mitosis of the originating cell (the originating cell is not represented in the tree). All links have the same standard length, while the colour of each link represents the division time of that cell, according to the colour scale shown below the trees: light-green indicates a short division time; dark-blue indicates a long division time (the mean division time across the whole dataset is about 20 hours). The elliptical thin lines separate different generations. All colonies have been followed up to the seventh generation, which means that the last divisions we observe are those between the $k = 6$ and the $k = 7$ generations; hence, we do not measure the division times of the $k = 7$ cells, which are therefore represented in grey. In some colonies all cells divide up to the seventh generation, giving rise to $2^7 = 128$ cells (20230113-07 - upper left), but in most colonies some inactive cells (G_0 or dead) emerge before. We represent a G_0 cell by a short black cap at the end of the link and a dead cell by a red dot at the end of the link. There is no node/mitosis at the end of an inactive link/cell, hence they do not have a division time and we conventionally represent them in black. It is important to keep in mind that this abstract representation of the lineage contains no information about the actual physical positions, and mutual distances, of the cells within the dish. **b)** To show the significant inter-colony heterogeneity of the topology, we report for each lineage in the dataset the number of inactive cells and the number of missing cells at the seventh generation. Both quantities have fluctuations that are almost as large as the mean. All lineage trees in the dataset are displayed in Fig.S1.

Within this representation of the trees, the bare backbone of a lineage – namely how cells are connected to each other independently of the colour of the links (i.e. independently of the division times) – is what we call the *topology* of the tree. We notice that the topology of a lineage is exclusively determined by how many inactive cells there are and by where they are positioned along the tree. Within the more naturalistic lineage representation in which each link has a length proportional to the division time (see e.g. [21]), different division times produce different structures, given the same topology. In other words, the overall structure of a colony is given by the interplay between these two factors: the topology (how inactive cells are distributed) and the kinetics (how fast/slow are the division times of the active cells). We aim here at disentangling the roles of these two factors, which is why we chose to be a bit pedantic and use the words 'topology' and 'kinetics', rather than 'structure'.

Lineage topology

We report a subset of our lineage trees in Fig.2a (all colony trees can be found in Fig.S1): upon a mere qualitative inspection, this figure shows a great diversity in the trees' topologies, confirming, at the lineage level, what previous studies have already established for many other parameters [8–10, 19–21], namely that there is a great *inter-colony* heterogeneity when studying populations of BMSCs. On the one hand, we find lineages that are perfectly round and whole, meaning that all branches of the tree arrive to the last recorded generation (Fig.2a - colony 20230113-07), and at the opposite side of the spectrum we find cases in which many branches are interrupted by inactive cells, giving rise to very broken trees (Fig.2a - colony 20230113-09). The topology of a lineage depends entirely on the number and on the positions on the tree of the inactive cells. Therefore, a first way to quantify the heterogeneity of the colonies is to measure for each colony the number of inactive cells, N_{inactive}; we find that this number has fluctuations almost as large as the mean, $N_{\text{inactive}} = 10.2 \pm 8.1$ (mean $\pm$ standard deviation), giving a relative fluctuation of 79%, a clear indication of the heterogeneity of the BMSCs lineages (Fig.2b).

Given a certain number of inactive cells, their effect in breaking the topology of the lineage depends on their generation: for example, a G_0 cell emerging at the second generation has the effect to cut a far larger number of cells at generation $k = 7$ compared to a G_0 cell at the sixth generation, which only cuts two. We can quantify this effect by counting the number of missing cells compared to a perfectly whole tree (which has 128 final leaves at $k = 7$). Naively one may expect that N_{inactive} and N_{missing} are simply proportional to each other, but this is not necessarily true: although the two quantities are broadly related (and in particular they are both zero in the perfectly whole trees), the value of N_{missing}, given N_{inactive}, depends on the position of the inactive cells; hence, they are actually independent parameters. We show in Fig.2b that the number of missing cells varies even more strongly than the number of inactive cells, $N_{\text{missing}} = 46.1 \pm 42.3$, with a relative fluctuation of 92%. Hence, topology is very heterogeneous also with respect of the variable N_{missing}, which reflects the great variability not only in the number of inactive cells, but also in the generation at which they emerge within the lineage.

Beyond the inter-colony heterogeneity, i.e. the strong variability of the structure from colony to colony, Fig.2a shows also that there are significant *intra-colony* heterogeneities, meaning that – if we look at one single lineage tree, in particular a rather broken one – we find branches with many interruptions and other branches that instead divide in a very balanced manner up to the largest recorded generation. In fact, it is exactly this intra-colony variability that is ultimately responsible for the inter-colony heterogeneity; in this sense, the former is more fundamental than the latter. Intra-colony heterogeneity was already noted with respect to cell shape, area

and other factors [19]. We will see later on that intra-colony heterogeneity – which is nothing else than an inter-branch heterogeneity – is associated to the hereditary character in the distribution of inactive cells.

A further observation that we can make by inspection of Fig.2a is that whole trees have overall a lighter colour, i.e. their active cells sub-population is on average faster, and *vice versa* broken trees are darker, i.e. their active cells sub-population is overall slower. This would be a non-trivial correlation, as the division time is a trait of the active cells sub-population, while the broken topology is caused by the inactive cells sub-population, and these two sets of cells are complementary. However, this observation should be made more quantitative, which requires analysing the statistics of the division times of active cells in all 28 colonies in the dataset and putting it in relation with the topology of the relative lineages.

But before doing that we must discuss a potential objection to how we defined topology. The topology of a given tree entirely depends on the number and distribution of the inactive cells; but while dead cells are unambiguously identified, G_0 cells (which are the largest majority of inactive cells) are less easily so. In our study we have employed a reasonable but still arbitrary operational definition of what a G_0 cell is, namely a cell that does not divide within a threshold time $t_c = 84$ hours. We must be sure that by changing the threshold t_c we do not produce trees with significantly different topologies. This objection is not pedantic: if the threshold time is chosen too close to the bulk of the division times of the population, we would mistakenly classify as G_0 cells that are not, and – consequently – we would produce lineage topologies that heavily depend on the arbitrary value of t_c. In order to know that we are not running this risk, we cannot limit ourselves to noticing that 84 hours is much larger than the mean division time of 20 hours; exactly because of the great heterogeneity of BMSC colonies, we must check for each single colony that the threshold time t_c that we are using to classify cells as G_0 is very distant not simply from the mean, but also from the bulk of the distribution of the division times of that colony. To do this, we therefore need to measure and characterise the division times, hence turning our attention to the colony kinetics. Apart from reassuring us about the G_0 classification issue, the study of kinetics will reveal some interesting correlation with the colonies' topology.

Colony kinetics

For each active cell within a colony we measure its division time, τ, with an accuracy of 15 or 20 minutes, depending on our time-lapse rate, which is quite acceptable, considering that the mean division time of human BMSCs is 20 hours (see Material and Methods for the precise description of the determination of τ). We then calculate for each colony the normalised histogram – i.e. the probability density – of the division times. In Fig.3a we report such histograms for the same colonies for which we report the lineages in Fig.2a (the complete set is provided in Fig.S1). The green vertical line in each histogram indicates the position of the threshold time that we use to define inactive G_0 cells ($t_c = 84$ hours). The value of t_c seems indeed to be quite far not simply from the mean, but from the whole bulk of the distribution, thus indicating that the definition of G_0 cells that we use is robust. We note that in order to evaluate faithfully the histograms of the division times it is essential to reconstruct the lineage up to a fixed generation ($k = 7$ in this study), rather than within a fixed observation time; indeed, fixing a maximum experimental time would cause the exclusion from the analysis of all the division times of the cells that divide after the observation time, significantly biasing the histogram towards lower values of τ [22].

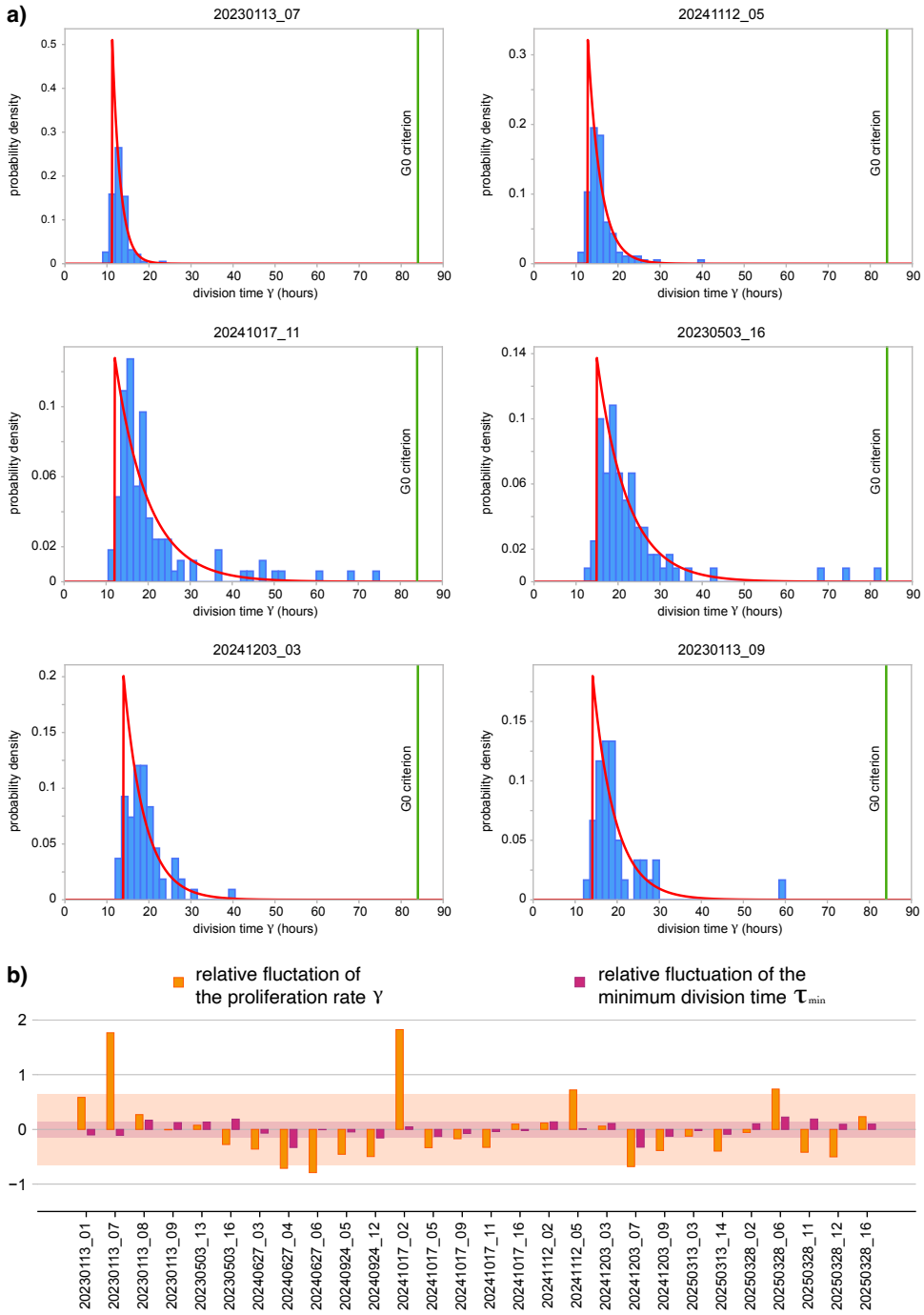

Fig 3. Kinetics – Statistics of the division times. a) We report the probability density (i.e. the normalised histogram) of the cells' division times, τ, for the same six colonies as in Fig.2. The vertical green line in each histogram indicates the 84 hours threshold that we use to define G_0 cells; in all colonies this threshold is well separated from the bulk of the division times, showing that the separation of the population into active and inactive sub-populations is a qualitative one. In all colonies there is a gap below which we find no division times. For this reason, a reasonably good fit of the data is given by the gapped exponential form (see text), which is characterised by a minimum division time $\tau_{\min}$ and a by a rate γ of decay of the exponential part of the function (red line). **b)** The same significant heterogeneity detected in the topology of the lineages is also apparent in the kinetics, in particular in the fluctuations of the rate γ; we report the relative fluctuations of the rate γ and of the minimum time $\tau_{\min}$. Interestingly, though, the minimum division time, $\tau_{\min}$, fluctuates much less than all other parameters, indicating that this part of the cell cycle is subjected to a smaller variability. All histograms of the division times in the dataset are displayed in Fig.S1.

The large τ tails of the histograms of the division times decay exponentially, a feature that would naturally arise in the context of simple branching models of cell proliferation, in which division events occur at a constant rate [31, 32]. However, a pure exponential form fits the histograms very badly, for reasons that are obvious from the inspection of Fig.3a: an exponential probability has its peak at $\tau = 0$, while all the experimental histograms show a clear and sharp gap at small division times, meaning that – even though the spread of the division times is quite large – no divisions are observed below a certain minimum value, $\tau_{\rm min}$. This kind of distribution of cell division times has been already observed in several systems, inspiring a class of models [33–35] where the probability distribution of τ is described by means of a gapped exponential form,

$$P_{\rm gap}(\tau) = \gamma\, \theta(\tau - \tau_{\rm min})\, e^{-\gamma(\tau - \tau_{\rm min})} \ . \tag{1}$$

The meaning of this distribution is quite simple: the division time τ (measured in hours) cannot be smaller than a minimum value $\tau_{\rm min}$ (the Heaviside function is defined as $\theta(x) = 1$ if $x > 0$ and $\theta(x) = 0$ if $x \leq 0$), hence $P_{\rm gap}(\tau)$ is 0 when $\tau \leq \tau_{\rm min}$, while beyond $\tau_{\rm min}$ a pure exponential decay with rate γ sets in; γ coincides therefore with the proliferation rate of the branching process associated to the colony's growth [31]; being the inverse of a time, γ has units of hours^{-1}. Finally, the factor γ in front of the r.h.s of (1) is required in order to have a normalized probability. With this gapped distribution the mean division time is given by,

$$\overline{\tau}_{\rm gap} = \tau_{\rm min} + \frac{1}{\gamma} \ , \tag{2}$$

where we use the symbol $\overline{\tau}_{\rm gap}$ to distinguish this value, which is obtained from a fit with the gapped distribution, from the experimental mean division time, $\bar{\tau}$, which is obtained by directly performing the average over all experimental division times of a given colony.

We fit function (1) to the division time data, hence finding the values of the proliferation rate γ and of the minimum division time $\tau_{\rm min}$ for each single colony in the dataset (more precisely, we determine γ and $\tau_{\rm min}$ by fitting the cumulative distribution of the division times, which is more reliable than the histogram). As we see from Fig.3a, distribution (1) fits reasonably well the data in most of the analysed colonies. Of course, more complicated functions can be envisaged, depending on the proliferation mechanism one considers (for example, the Erlang distribution has been used in Ref. [36], derived from a representation of cell proliferation as a Markov process). Here, we use one of the simplest forms, which seems to capture the experimental distributions of the division times in a reasonable way: there are no cell cycles shorter than a minimal duration, and above such threshold divisions occur at constant rate.

We report the values of the two fit parameters, $\tau_{\rm min}$ and γ, for each colony in the dataset in Fig.3b, whence we notice something interesting: while the proliferation rate γ fluctuates rather strongly from colony to colony ($\gamma = 0.19 \pm 0.12$ hrs^{-1}; relative fluctuation: 63%), thus abiding to the usual pattern of strong inter-colony fluctuations, the minimal division time, $\tau_{\rm min}$, is significantly more stable ($\tau_{\rm min} = 12.6 \pm 1.8$ hrs; relative fluctuation: 14%). This fact, together with Eq.(2), suggests that the mean division time of a certain colony is made up of two different contributions: a quasi-deterministic part, given by $\tau_{\rm min}$, which is roughly the same for all colonies – and therefore for all cells – and a stochastic part, given by the inverse proliferation rate, $1/\gamma$, which strongly depends on the colony. This analysis cannot tell how these two contributions are mutually located along the cell cycle, nor whether there is any temporal order between them. It merely indicates that there are certain

processes within the cell cycle whose total duration $\tau_{\min}$ is very stable from cell to cell and cannot be compressed, while the remaining processes building up the full cell cycle have a strongly fluctuating duration. This result is consistent with what is known about the cell cycle progression, namely that stages S, M and G_2 are quite stable in duration, while G_1 fluctuates much more [23, 33]. In particular, several recent studies confirm that the G_1 phase is the most variable one, both in embryonal and somatic stem cells [25, 37], and suggest that such variability is associated to proliferation regulation and cell fate determination [25, 38, 39]. Our findings corroborate and expand this scenario, by showing that the variable phase of the cell cycle, whose duration is given by $1/\gamma$, also fluctuates coherently from colony to colony.

Considering that the colonies in our dataset are derived from cells coming from 6 different donors, of different age and sex, and that cells were plated at different passages (P0, P1, P2 – see Table S1), it is natural to ask how much of the observed variability in the topology and in the kinetics depends on these factors. Interestingly, the data show that the degree of heterogeneity within one experiment (same donor, age, sex, passage) is approximately as large as the heterogeneity between different experiments; indeed, it may happen that two different cells from the same donor, cultured within the same experiment on the same plate, give rise to two completely different colonies: for example, lineage 20230113-07 has no inactive cells and is perfectly whole, while lineage 20230113-09, from the exact same experiment, is highly broken (see Fig.2a). In Fig.S3 we present a comparison of the mean division times of all colonies in our dataset, detailed for experiment, donor, age, sex and passage. Even though we cannot completely exclude some *very* weak correlation between kinetics and passage (Spearman correlation $\rho = 0.33$, albeit not statistically significant, P-value = 0.09), the intrinsic variability within each single experiment seems to largely dominate the overall heterogeneity in the data.

The correlation between topology and kinetics

Once we have established that the structure of the lineage trees is robust, in that it does not depend on the threshold t_c that we employ to define G_0 cells, we can quantify the observation previously made by inspection of Fig.2a, namely that broken trees seem to correspond to slower colonies and *vice versa*. To do this, we analyse the relation between the total number of inactive cells of each lineage, N_{inactive}, and the mean division time of the colony, $\bar{\tau}$; notice that these are both quantities directly measured from the data, with no fit involved in their determination. The result is shown in Fig.4a: despite the scatter, we find a very strong and significant correlation between the number of inactive cells and the mean division time (Spearman correlation coefficient $\rho = 0.841$, P-value $< 10^{-6}$ – see Material and Methods for the precise definition of P-value that we use). Such sharp correlation does not depend on the parameters we choose to characterise topology and kinetics; instead of the total number of inactive cells we can use the number of missing cells, N_{miss}; similarly, instead of the mean division time (that derives directly from the data), we can use the inverse proliferation rate, $1/\gamma$ (which derives from a fit to Eq.(1)). In Fig.4b,c,d we show that all these correlations are strongly significant, meaning that the connection between lineage topology and colony kinetics is robust: broken trees indeed correspond to slowly proliferating colonies.[2]

[2]Notice that the *positive* correlation between the number of inactive cells and the mean division time can only hold for colonies large enough to have some cells at generation $k = 7$ (as those included in this study); if, on the contrary, we selected very small colonies where *all* cells are G_0 (no cells arrive at the seventh generation), we would enter a qualitatively different regime where N_{inactive} would be *proportional* to the size of the colony and where N_{missing} would always be equal to 128. If one is interested in that regime, other metrics should be used to describe the topology of the tree.

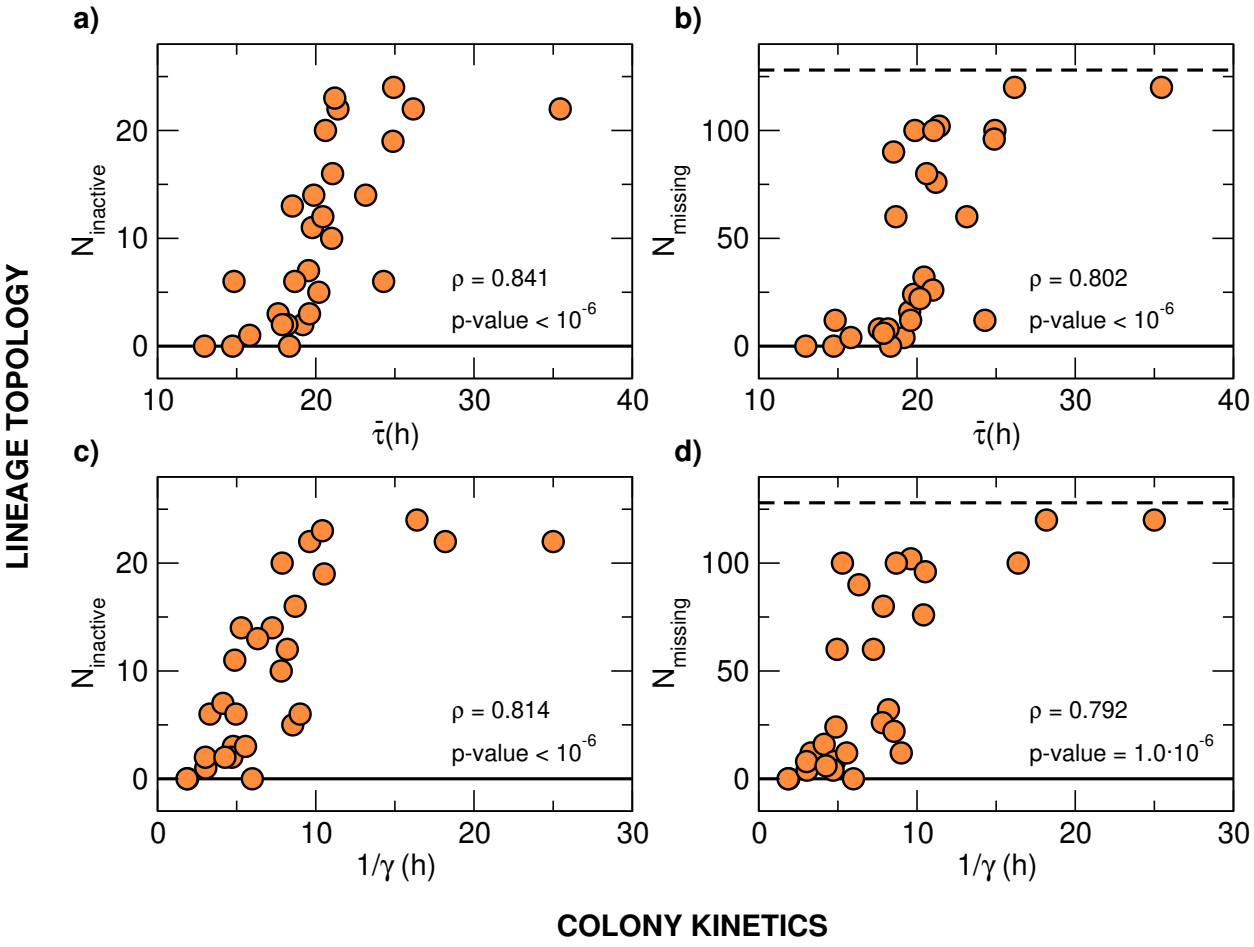

Fig 4. The correlation between topology and kinetics. a) We plot the number of inactive cells of each colony, N_{inactive} – a characterization of the topology of the lineage – as a function of the mean division time of that colony, $\bar{\tau}$ – an indicator of the kinetics. It is important to remember that inactive cells do not have a division time, hence only active cells contribute to $\bar{\tau}$, so that these two quantities come from well-separated sub-populations of cells. The Spearman correlation between N_{inactive} and $\bar{\tau}$ is very significant, with correlation coefficient $\rho = 0.841$ and P-value $< 10^{-6}$. **b)** Another characterisation of topology is given by the number of missing cells at generation $k = 7$, N_{missing}, which happens to be also strongly correlated to the mean division time, $\bar{\tau}$ (Spearman $\rho = 0.802$, P-value $< 10^{-6}$). The dashed line represents the maximum number of missing cells, namely $2^7 = 128$. **c-d)** The rate γ extracted from the fit of the division times histograms is another indicator of kinetics. We plot N_{inactive} and N_{missing} vs $1/\gamma$ (which has the physical dimensions of a time) and find in both cases an excellent correlation ($\rho = 0.814$, P-value $< 10^{-6}$ and $\rho = 0.792$, 1.0×10^{-6}, respectively). We conclude that all indicators of topology are correlated with all indicators of kinetics in the same strong way: colonies with more broken lineage trees have a slower kinetics, suggesting that the mechanisms regulating the emergence of inactive cells are also involved in the regulation of the duration of the cell cycle of active cells.

Results in line with the correlation between topology and kinetics that we find here have been reported before by other groups working on BMSC lineage tracing. In Ref. [19] it was found that the division time of parents of cells that both divided was shorter than the division time of parents of cells that both stopped dividing, with mixed dividing-not-dividing pairs in between. In Ref. [21] it was found that cells belonging to slow-dividing progenies had more senescent daughters on average than cells belonging to fast-dividing progenies, where slow-dividing progenies were defined as those producing less than 8 cells at day 4 and fast-dividing progenies were those producing more than 16 cells at day 4. Both these observations were performed at the single-cell level and were based on binary (or at most ternary) classifications of the kinetics. Fig.4 shows that the correlation between topology of the inactive cells and kinetics of the active cells remains strong at the collective level of the entire colony and that it is robust against unfolding the binary slow-fast classification into the full continuous spectrum of the mean division times.

Before discussing the possible meaning of the correlation between kinetics and topology, let us emphasise that these two traits are determined by two phenotypically *well-separated* complementary sub-populations: the tree topology is uniquely determined by the number and distribution along the lineage of *inactive* cells, while the kinetics is exclusively determined by the division times of the *active* cells, which are the only ones actually proliferating. Although it may seem tautological, it is worth reminding that the inactive cells of a colony do not participate to the cell cycle and therefore do not contribute to the mean division time of that colony, which is solely determined by the active cells; conversely, the division times of the active cells bear no direct information about the lineage structure of the inactive cells of a given colony.

Although the correlation between topology and kinetics seems rather intuitive, we should nevertheless be careful with its interpretation. A possible (wrong) argument to expect a correlation between broken topology and slow growth would be the following: if a colony is slow, the divisions times of its cells are on average very large, so that once in a while a cell may divide after an exceedingly long time, larger than the threshold t_c that we use to tag cells as G_0. Hence, one could argue that the G_0 tag we assign does not correspond to a *qualitatively* different cell state, but it is just a *quantitative* epiphenomenon of having chosen an arbitrary threshold t_c. Were this the case, the correlation between the number of inactive cells (which is primarily determined by the G_0 cells) and the division time (which is determined by the active cells) would be trivial – in fact, even tautological – as both quantities would derive from the *same* actual probability distribution of division times, which we would be artificially separating into two parts: the active cells, $\tau < t_c$, and the inactive cells, $\tau > t_c$.

This argument is not consistent with the data. We have already seen that the threshold t_c that we use to define the G_0 state is well separated from the bulk of the distribution times, which makes the argument above already unsound. But we can easily reject the argument at a more quantitative level. Given a certain colony, we can use the probability distribution $P_{\rm gap}(\tau)$ fitted to the actual experimental histogram of the division times of that colony (Fig.3a), and calculate the probability to find a cell that has a division time larger than t_c, a cell that would therefore be erroneously tagged as G_0 in our experiment, according to the argument above. This probability is given by,

$$p_{G_0} = e^{-\gamma(t_c - \tau_{\rm min})} \ . \tag{3}$$

Using the actual experimental value of $t_c = 84$ hours and the fitted values of γ and $\tau_{\rm min}$ in each one of our colonies, we find that this probability is always extremely small, ranging between 10^{-17} to 10^{-2} (see Table S1); this means that if in each colony we extracted the cell division times using its own probability and tagged as G_0 all cells with $\tau > t_c$, we would obtain a number of G_0 cells that is approximately equal to

$p_{G_0} \times 128$, which yields *zero* in 25 out of 28 colonies, in stark contrast with their actual total number of G_0 cells, which is 225; in fact, even in the three colonies in which $p_{G_0} \times 128$ is non-zero, we would obtain 7, 2 and 1 G_0 cells, instead of the actual 22, 18, and 22 G_0 cells that those colonies actually have. We conclude that those cells classified as G_0 in our experiments are *not* merely the very slow cells; the inactive cells sub-population is thus a *bona fide* qualitatively different group from that of the active cells. Therefore, the tautological explanation of the correlation between topology and kinetics does not stand.

Yet, what the data in Fig.4 clearly show is that some non-trivial underlying correlation between the active and inactive phenotypes *does* exist, which is telling us something about how these phenotypes are determined. The correlation between broken topology and slow growth suggests that the factors regulating the duration of the cell cycle are also involved in the determination of the non-proliferative state. This conclusion is consistent with the proteomic profiling of BMSCs colonies mapped out in Refs. [40] and [41]; in those studies, single-cell derived colonies were classified as slow-growing or fast-growing, depending on the time taken to reach 20 population doublings, and it was noted that slow colonies had limited differentiation potential (unipotential), while fast colonies had tripotential differentiation capacity. The proteomic analysis of 170 proteins within these two different groups showed that 3 proteins had increased abundance in fast-tripotential colonies, while 8 proteins had increased abundance in slow-unipotential colonies [41]. Among these differently-expressed proteins in the two groups, of particular interest was the enhanced expression of calmodulin (CAM) and tropomyosin (TM) in *fast* colonies: CAM blocks Fas-mediated apoptosis [42] and more generally CAM and TM act as modulators during cell proliferation. On the other hand, the over abundance of caldesmon (CAD) and Annexin-I in *slow* colonies was equally relevant relevant, because CAD acts as a regulated break to cytokinesis, while over-expression of Annexin-I reduces cell proliferation [41]. Therefore, proteomic profiling indicates that fast-growing colonies express factors that may reduce the number of cell deaths (although not necessarily of cells entering the G_0 phase) and increase proliferation, whereas slow-growing colonies have a larger abundance of proteins potentially depressing proliferation. This evidence is broadly consistent with the correlation between inactive cells topology and active cells kinetics that we find here, suggesting that some of the factors discovered in Ref. [41] may also be involved in the triggering of the G_0 state of BMSCs. Still, being 2^{20} larger than one million cells, the slow-growing vs fast-growing classification given after 20 doublings in Ref. [40] employs a time window *hugely* longer than that of our experiments, hence one should be cautious in the comparison: if the consistency between our results and those of [40] suggests that the long-term ($k = 20$) proliferation potential is already detectably in the very early generations ($k = 7$), specific experiments directly comparing the short-term to the long-term behaviour of individual colonies should be performed to validate such promising connection.

To conclude this Section, let us note that no matter the relevance of *in vitro* experiments – like all lineage studies necessarily are – the gold standard to characterise the differentiation capacity of BMSC colonies is *in vivo* transplantation. In Ref. [9] colonies of BMSCs were transplanted into immunocompromised mice to determine the bone-forming capacity of these colonies and assess the correlation between this capacity and their proliferation rate; although the kinetics was not found to be strictly predictive of osteogenesis in that study, a certain weak correlation between proliferation rate and bone formation *in vivo* was anyway found. A subsequent study, Ref. [10], distinguished between colonies that upon *in vivo* transplantation formed fibrous tissue, those that formed bone, and those that formed

bone/marrow organ, where only this third class was deemed multipotent; however, in that study the proliferation rate and its possible correlation with multipotency was not assessed. Therefore, although it seems that high proliferation rate and hence a faster kinetics overall – which in turn implies a smaller number of inactive cells – may be positively correlated to the osteogenic potential, more *in vivo* studies are needed to correlate kinetics to *bona fide* multipotency.

Inheritance

We have already noted that inactive cells determine the topology of a lineage tree through both their number and their position within the tree. The position of inactive cells is characterised by two parameters: generation and branch. For example, concerning the first: the effect of a G_0 cell on the topology is very different if it is located at generation $k = 2$ or at $k = 6$, as in the first case the number of final missing cells due to that single G_0 will be much larger. As this simple example shows, the distribution of inactive cells across different generations impacts mostly on the different types of cell counters, in particular on the missing cells. We have already seen in Fig.4 that both N_{inactive} and N_{missing} are strongly correlated to kinetics, hence we conclude that the growth rate of the colony is correlated to topology through the number of inactive cells *and* their position across generations.

The branch placement of inactive cells, though, has a subtler role. Let us consider, for example, lineage 20241017-11 in Fig.2a: there is clearly something peculiar about the distribution of the inactive cells in this tree, as they seem clustered within the same few branches on the south-west side of the lineage in a definitely non-random way; a similar observation could be made for lineage 20230503-16, where inactive cells are mostly concentrated in the west wing of the tree. This seems a general trait: in most lineages we observe significant imbalances of the number of inactive cells between branches, indicating that the emergence of inactive cells is more likely in some branches than in others. If we follow a branch with many inactive cells up along the lineage, clustering suggests that at some point during proliferation a factor linked to the probability of emergence of inactive cells changed, making one cell more prone to giving rise to inactive cells within its progeny. In other words, the non-random branch-to-branch distribution of inactive cells seems to be revealing something about *inheritance*. The probability of emergence of inactive cells is the product of the complex interplay between the environment (extrinsic factors) and the cell regulatory processes (intrinsic factors); this second element is the one potentially inherited from mother to daughter. Hence, the topological evidence seems to provide information about how a change in the probability of emergence of inactive cells is inherited.

We will now put this hypothesis to a quantitative test. The most important effect of the presence of inactive cells on the lineage is that all cells that would have been born as their progeny are instead missing; hence, the number μ of missing cells at generation $k = 7$ is a good indicator of the impact of inactive cells on a certain branch. Each mitosis m generates two branches, a left branch and a right branch, and each one of these branches comprises a has number of missing cells, $\mu_m^{(L)}$ and $\mu_m^{(R)}$; we then define the *inactivity imbalance* of mitosis m as the difference between the right-left numbers of missing cells (see Fig.S4a),

$$I_m = |\mu_m^{(R)} - \mu_m^{(L)}| \ , \tag{4}$$

where we use the absolute value because the actual left-right order of the two branches after each division is arbitrary (a tree with left and right branches exchanged represents exactly the same lineage). At variance with other measures of tree imbalance, such as the Colless index [43, 44], we do not consolidate the imbalance into

a sum over all nodes of the tree. This is crucial: from the point of view of inheritance, a large inactivity imbalance at a few nodes is *not* the same as a buildup of small inactivity imbalances scattered over many nodes; if there were no inheritance, but just a uniform small probability of emergence of inactive cells, the tree would anyway show small random imbalances at most nodes. Instead, inheritance is signalled by an exceptional event, namely by a large imbalance concentrated on one node, or a few nodes, signalling a difference between the two daughter cells generated at that mitosis, a difference that is passed to their progenies (see Fig.S4b). Therefore, we need a quantity able to detect when there are atypical values of the inactivity imbalance, I_n, and when – on the other hand – the imbalances are all more or less the same. The tool explicitly designed to do this is the *entropy*, which is quite generally defined as,

$$S = -\sum_m \left(\frac{I_m}{\sum_n I_n} \right) \log \left(\frac{I_m}{\sum_n I_n} \right) \ , \tag{5}$$

where the sums are extended over all mitosis in the lineage.[3] The entropy S is high when the inactivity imbalances I_m all have approximately the same value, so that we receive no particular information about the occurrence of an inherited change at any mitosis in the lineage; on the other hand, entropy is low when there are few large imbalances concentrated on a handful of mitosis, as in that case we have reliable information that an inherited change occurred at those mitosis (see Fig.S4a for an actual calculation of all imbalances and their relative entropy). In short – and quite coarsely – high entropy means low evidence of inheritance, while low entropy means high evidence of inheritance.[4]

The entropy of a tree depends not only on the distribution of inactive cells, but also on their total number, as well as on the overall size of the tree. Therefore, it is hard to establish what are high or low values of S on an absolute scale; but fortunately we do not need this, because we are not attempting to compare different biological lineages using S. Instead, we want to know how likely it is to obtain the same entropy as a specific biological lineage in a tree where all inheritance relations between mother and daughters have been severed; in other words, we want to compute the P-value of the entropy we measure vs the null case of a completely *non-hereditary* tree. This task is easily achieved by randomly scrambling the actual biological tree (see Fig.5 top, and Fig.S4b,c): at each generation k, all cells are randomly reshuffled (within that same generation) and when two cells are exchanged, so are the branches/progenies generated by those two cells; then we move to generation $k+1$ and we scramble again, and so on. Notice that in this way all hereditary connections are randomised, and yet the total number of inactive cells at each generation remains the same; therefore, the scrambling procedure maximises the entropy by erasing all possible hereditary information, thus producing a completely non-hereditary tree, which however has the same number of inactive cells per generation as the biological one (Fig.5, centre and Fig.S4c). The scrambling procedure is repeated a million times for each biological tree and the P-value is given by the fraction of scrambled trees that happen to have $S_{\text{scrambled}} \leq S_{\text{biological}}$, namely by the probability that a completely non-hereditary tree gives an evidence of inheritance larger than or equal to the biological tree (notice that in this way the highest significance corresponds to $\mathrm{P} < 10^{-6}$).

[3] As usual with the definition of entropy, $x \log x = 0$ for $x = 0$; hence, mitosis with zero imbalance do not contribute to any of the sums in S.

[4] It is worth noting that the entropy defined in (5) is essentially the same as the Theil index, T, of economic inequality [45], namely, $T = \log \mathcal{N} - S$, where $\mathcal{N}$ is the total number of entries. Notice that the normalised quantities $I_m/(\sum_n I_n)$ do not have an obvious frequentist interpretation as probabilities and therefore we should not blindly rely on the interpretation of the entropy S in the context of Shannon information theory.

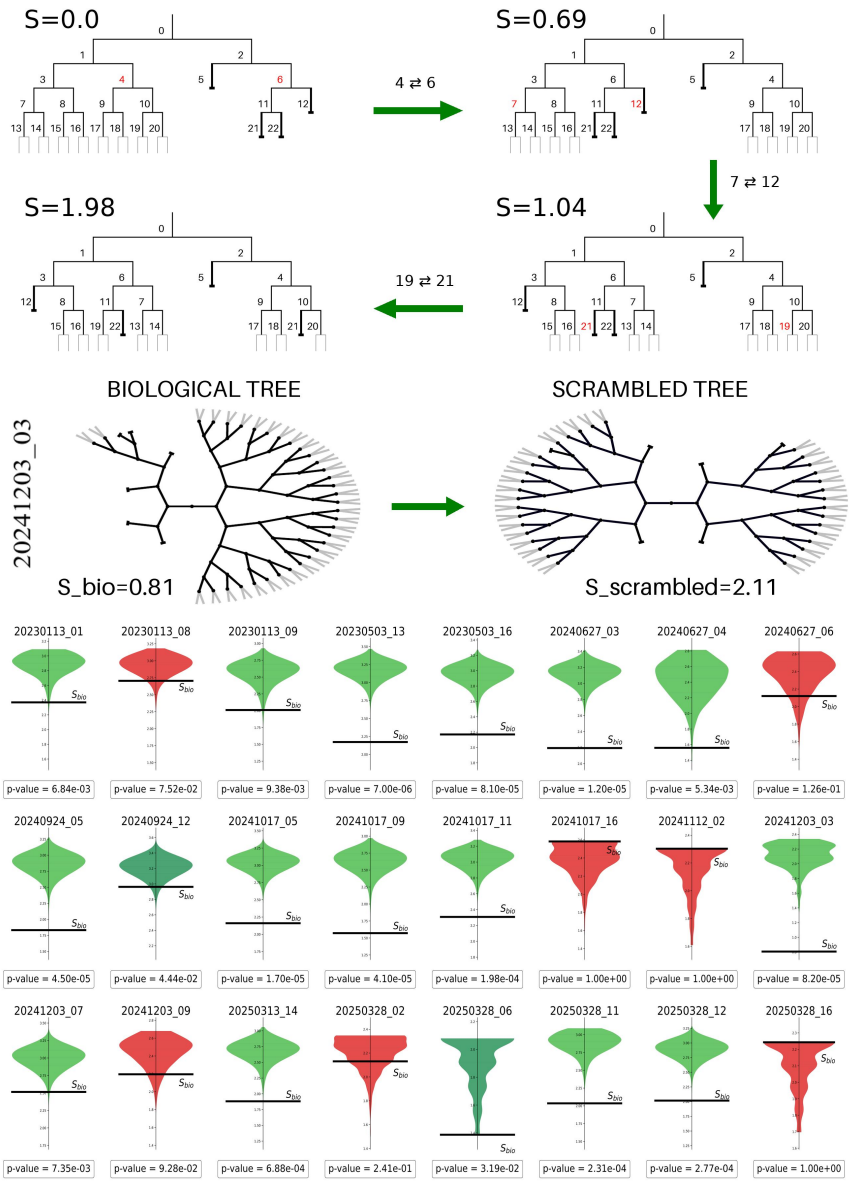

Fig 5. Scrambled trees and inheritance test. (Top) In the upper panels we illustrate – by using a fictitious tree – the process of lineage scrambling that we use to run the inheritance test. This tree is designed to have a clear clustering of G_0 cells on the right wing, and therefore a strong inheritance signal (i.e. a low entropy, in this case the lowest, $S = 0$). Cells at the same generations are randomly swapped, together with their progeny, and this procedure is repeated recursively at all generations; with each step of scrambling the entropy grows, and in the end a tree is obtained with a much higher entropy than the original one ($S = 1.98$), hence a much weaker inheritance signal. Technically, the scrambling procedure of one tree is complete once a random permutation of all cells of each generation is performed. **(Middle)** We report here a real biological lineage (colony 20241203-03); this tree has a strong concentration of G_0 cells, and therefore of missing cells, in the west wing of the lineage; in this three, the imbalance is generated at the very first mitosis in the lineage, the central node of the tree. Instead, one of the (many) scrambled versions of the biological tree has G_0 cells and missing cells distributed evenly across all branches. The entropy of the biological tree is $S_{\text{bio}} = 0.81$, while the entropy of the corresponding scrambled tree is $S_{\text{scrambled}} = 2.11$. When we produce 10^6 scrambled versions of 20241203-03, we *never* find $S_{\text{scrambled}} < S_{\text{bio}}$ and only a few times (over a million) we find $S_{\text{scrambled}} = S_{\text{bio}}$; this means that the probability that the entropy is so small in the biological case by pure chance is extremely low - we find a P-value of 8.2×10^{-5} (see Table S1) - making the inheritance test for colony 20241203-03 highly significant. **(Bottom)** The result of the inheritance test is reported for all colonies in the dataset for which the test can be run. For each colony, the violin plot represents the probability distribution of the entropy for the set of 10^6 randomly scrambled trees, while the black line is the value of the entropy of the non-scrambled biological tree. Therefore, the P-value is the total area (i.e. probability) of the violin plot which lies below the black line. Bright green: high significance of the inheritance test (P-value < 0.01); dark green: fair significance of the inheritance test (P-value < 0.05); red: non-significant inheritance test (P-value > 0.05).

Results about the inheritance test on our BMSC colonies are reported in Fig.5 (see also Table S1). We have 28 colonies in total in our dataset; in 4 colonies the test cannot be run because they have either zero or one inactive cell, hence the scrambling produces always the same tree. Of the 24 colonies for which we can run the inheritance test, 17 (71%) have lineages with a significant hereditary character: of these, 15 pass the test with high significance (P-value < 0.01) and 2 pass the test with fair significance ($P < 0.05$). On the other hand, in 7 colonies out of 24 (29%) the inheritance test gives a non-significant result ($P \geq 0.05$); these non-significant cases are mostly given by colonies with very small number of inactive cells, for which the inheritance test – which is based on scrambling many times the positions of the inactive cells – is not expected to be very effective in the first place; in just one colony (20240627-06), the inheritance test gives a non-significant result despite its large number of G_0 cells (interestingly, with its very long mean division time, this colony is also a slight outlier in the topology vs kinetics plot of Fig.4). It is important to stress here that a non-significant test does not necessarily imply that there is no inheritance at work, because a negative result is equally obtained when there is no change in the probability of emergence of inactive cells along the lineage: the lack of variation in the expression of a character makes inheritance undetectable. Summarising, the overall outcome of the inheritance test leads us to conclude that the topology of the largest majority of human BMSC colonies cannot be attributed to random variations in the positions of inactive cells across different branches, thus indicating that the processes responsible for regulating the probability of emergence of inactive cells have a strong hereditary character.

It must be noticed that if we observed more complex regulatory factors, it could turn out that a lineage that did not pass the inheritance test at the bare topological level, still results hereditary according to these other factors, and indeed we expect this to be the case. But we cannot help noticing that calculating the entropy and its P-value is easy and quick, as one needs nothing but the bare topology of the lineage. Hence, it seems lucky – and interesting – that most BMSC colonies display a sharp hereditary distribution of inactive cells already at such a fundamental and simple level as the bare lineage topology. It is important to stress here that an experiment that does not respect a sharp G_0 criterion (for example, because proliferation is followed up to a fixed maximum experimental time), may yield a total number and a distribution of inactive cells which is severely biased [22], making the inheritance test unreliable.

The evidence of inheritance detected here is very unlikely to be of genetic origin, because the relatively short timescales of the experiment and the low number of generations makes it improbable that the cell-to-cell variations that we observe (and use to identify inheritance) are due to genetic mutations [8, 46]. Instead, our results point to inheritance of the epigenetic modifications or, more generally, of the changes of transcriptional and regulatory factors.

Is it possible that the clustering of G_0 cells on the same branches of the lineage tree, which we interpret as an hereditary character, is in fact an epiphenomenon of spatial correlation in the physical space of the dish? Namely, is it possible that chemicals/nutrient heterogeneities, local crowding, or other spatial factors might influence the propensity to enter the G_0 phase in a way that is then reflected in the lineage topology? We recall that proximity in the physical space does not imply proximity on the tree, hence it is unlikely that clustering on the tree is produced by the fact that these cells are actually close to each other in the dish. More precisely, points that are close on the tree tend also to be close in physical space, since cells derived from a common close progenitor have less time to move and separate in space than cells derived by far progenitors; but the crucial point is that – as shown in Fig.S2 – the *vice-versa* is not true, namely points close in physical space are not necessarily

close in the lineage. For the sake of argument, let us assume that there exist on the Petri dish a localised spot of size R where spatial factors promote the G_0 state; if a mitosis occurs in that G_0-promoting spot and if the colony is already quite crowded – and hence mobility is limited – it is likely that also the two daughters' mitosis will occur in that same spot. If these were the only mitosis taking place in the spot, this could explain the clustering that we observe in the lineage trees without the need to invoke an hereditary mechanism. However, this is not what happens, as clearly illustrated in Fig.S2: the range of topological distances between the points belonging to a physical region of size R is *very* wide; even a physical spot of a few hundred pixels, which is about the size of a cell, has a typical size on the tree of over 7 links, and it is very likely to find within this spot points with distance on the tree of up to 12 links, which is the maximum amplitude of any lineage. This result indicates that any hypothetical G_0-promoting spatial spot would typically contain also many mitosis with *large* topological distances from each other, which would in turn imply that the G_0 cells created by the anomalous spot would be found all over the tree and not simply clustered within some branches, which is instead what we observe. We conclude that the G_0 clustering we discovered on BMSC trees is very unlikely to be of spatial origin and that the hereditary explanation is the most plausible one.

The role of inheritance in clonal cell replication has been studied in several different contexts and regarding many different types of characters [46–51]. In this respect, our finding that inheritance plays an important role in the distribution of inactive cells is not unexpected. It is known (see, for example, Ref. [51]) that cells switch between molecularly and phenotypically distinct states as they proliferate through repeated divisions; it is precisely this cell state that is passed to the progeny in a hereditary way, regulating cell fate decisions and progeny differentiation. Therefore, it is essential on one hand to characterise as precisely as possible cell states – and to determine what states are phenotypically distinct – and on the other hand to understand how cell states evolve along a mitotic lineage. Modern techniques in single cell profiling allow to measure the whole transcriptome (single cell RNA-seq), as well as proteomes and metabolic signatures, and to characterise the cell state in a very detailed way. Moreover, much effort has been devoted recently to characterise the multi-dimensional space of cell states (the 'state manifold' or 'transcriptional landscape' [52]). At the same time, novel techniques for large scale lineage tracing have been developed. The final aim is to combine the two analysis to identify well-defined cell states and the transitions among them, as well as to establish an hereditary lineage hierarchy of cell state transitions. Particularly promising to this end are the new barcoding lineage tracing methods, which allow to acquire both types of information simultaneously, by inferring lineage relationships and cell state information from end-point measurements [53–56]. Barcoding lineage techniques are extremely powerful, although they still present limitations in terms of applicability to human stem cells [57] and accuracy in lineage reconstruction [52].

The approach we have adopted here to cope with the interplay between inheritance, lineage tracing and cell state is much more simplified and somehow complementary to the methods described above. Cell states are defined in terms of a simple phenotypic trait, being active or not, which is certainly a drastic projection of the much wider information contained in the whole transcriptome. On the other hand, the mitotic lineage tree is reconstructed very precisely starting from a single progenitor, and the characterisation of inheritance is quite sharp. This accuracy, combined with the clear classification of cell identities, allows to pinpoint how lineage heterogeneity and topology are linked to the inheritance of certain cell traits during proliferation.

Conclusions

By conducting time-lapse microscopy on a set of 28 non-overlapping single-cell-derived colonies of human BMSCs, we discovered a sharp correlation between lineage topology, which is determined by the sub-population of inactive cells, and colony kinetics, which depends entirely on the division times of the sub-population of active cells: lineages that are broken by the presence of many inactive cells (typically in their G_0 state), are also characterized by an active sub-population with a slower proliferation rate, and *vice-versa*. This correlation connects a binary state of the cell (active or not) to a variable depending in a continuous way on the proteonomic expression (the division time), a phenomenon that does not depend on the criterion used to tag a cell as G_0, because the two sub-populations (active vs inactive) are well-separated from each other at a qualitative level.

As it happens with many other traits of BMSC colonies, both the number of inactive cells and the mean division time of active cells – as well as other quantities characterising topology and kinetics – are strongly heterogeneous. The interesting consequence of having found a strong correlation between topology and kinetics, however, is that such correlation reduces the number of potential *independent* factors at the origin of the heterogeneity of both traits, hence partly reducing the complexity of the problem. By establishing a mutual dependence of the fluctuations of the number of G_0 cells and the fluctuations of the division times of active cells, we effectively turn what seemed independent random variations, into a *function*, with a underlying single causal factor; this factor needs to explain why, within the same clonal cell population, a longer cell cycle time is associated to an increase of the probability to enter in the G_0 state, instead of finding two independent mechanisms that increase the variability of G_0 cells and of slow cells.

If correlation between topology and kinetics reduces the number of independent causes of variability, the second trait that we study – inheritance of the probability to enter the G_0 state – reduces the number of independent changes in the lineage, namely the number of occasions along the colony proliferation where such variability may have arisen. This is because, once a modification in the expression of some transcription factor determining the G_0 state occurs in a cell after some mitotic event, this modification is inherited by the progeny of that cell, hence shaping the topology of the tree in a clear hereditary way. Note that, even though we did not measure the hereditary nature of the division times, the chain of correlation we have established suggests that also the fluctuations of the division times are subject to some inheritance rules. The test of inheritance we have developed relies on the entropy of the imbalance of inactive cells, but one could introduce other metrics to perform an inheritance test of the lineage; the entropy-based method has the virtue to be simple, fast and quite direct, but it is certainly worth exploring more structured tools.

Compared to other studies, where genetic expression is explicitly monitored by direct measurements (proteomics, transcription factors, etc.), and even compared to other lineage studies that include several more cell features (e.g. cell area, mobility, positions, etc), our analysis is definitely more basic. By focusing solely on the bare topology of the lineage tree (which is determined exclusively by the distribution of inactive cells) and on the division times of the active cells, we are missing important information about the great diversity of the cellular mechanisms actually linking topology to kinetics. On the other hand, although the information coming from gene expression is indeed incredibly rich, it may also be somewhat difficult to organise into concise conclusions; besides, its experimental determination can hardly be complete, nor extremely precise. Within the simpler framework developed here, one can instead draw clear conclusions, especially because this type of study can be conducted in a complete and precise way: we have an extremely accurate lineage tracing, we measure

the division time of all active cells, we only select single-cell derived colonies, we only monitor colonies that do not interact/overlap with each other, we analyze each colony up to the same generation. There is always a trade-off between complexity/incompleteness/inaccuracy on the one hand, and simplicity/completeness/accuracy on the other hand, and inevitably one has to lose something to gain something. Clearly, our study leans on the latter part of the spectrum, where robust statistics and simple but reliable data can pin-point basic yet solid correlations. Of course, ideally one would like to unify and exploit both levels of investigation, i.e. to have an accurate and complete lineage of a large isolated colony, associated to a complete proteonomic profiling of that same colony. Although huge efforts and considerable progresses have been made in recent years in this direction, a degree of incompleteness and inaccuracy inevitably remains, thus making simpler studies like the present one potentially still useful.

Materials and Methods

Cell source

Human bone marrow stromal cells (BMSCs) were isolated from bone samples harvested from healthy subjects undergoing elbow orthopaedic surgery through procedures approved by the local ethical board (Rif. 5313 Prot. 387/19) and upon informed consent of the patients. Bone fragments were collected in Minimum Essential Medium with α modification (α-MEM, Merck, Saint Louis, USA) supplemented with 1% Penicillin/Streptomycin (P/S, Merck) by the surgeon and transferred to the laboratory where the isolation of the cells was performed. Bone pieces were minced and washed with phosphate-buffered saline (PBS) in order to allow the release of bone marrow cells. Cell suspensions were collected in culture medium consisting in α-MEM supplemented with 20% Fetal Bovine Serum (FBS, Thermo Fisher Scientific, Waltham, USA), 1% P/S and 1% L-glutamine (L-gln, Merck) and counted on a hemocytometer. Cells were cultured at the density of $1 - 20 \times 10^3$ nucleated cells/cm^2 at 37° C, in a 5% CO2 atmosphere. The remaining cells were cryopreserved at the cell density of $1 - 3 \times 10^7$ total cells (including red blood cells) per mL of Bambanker Serum-free cell freezing medium (Nippon genetics Europe) for subsequent uses.

Cell planting and seeding density

After 24 hours of culture, non-adherent bone marrow cells were removed and adherent BMSCs were grown as P0 until confluency of the colonies (10-14 days). Confluent BMSC colonies were detached using 0.05% trypsin-EDTA (Merck), counted and plated as P1. The same procedure was applied to establish P2 cultures. Time lapse experiments were performed with either P0, or P1 or P2 cultures (see Table S1). P0 experiments were performed with freshly isolated BMSCs. P1 experiments could be established either starting from freshly isolated cells, or from cryopreserved bone marrow cell suspensions. P2 cultures were established starting from cryopreserved bone marrow cell suspensions. To prepare the cultures for time lapse experiments, cells were plated at the density of 50 cells/dish in 35 mm μ-Dish Petri, model 81156 (Ibidi, Gräfelfing, Germany). The culture medium was filtered through a 0.22 μm syringe filter to prevent the presence of serum residues in the culture. Two identical dishes were generated, one starting the time-lapse experiments in the microscope stage top chamber incubator, while the other was incubated in the standard incubator (Heracell, Heraeus) as positive control of cell growth. After 6 hours, cells in the two dishes were checked to verify their attachment, and one of the two dishes was inserted

in the microscope to start the time-lapse imaging, while the second dish becomes the control (see below). At this stage, the actual number of cells found in the observational area of the μ-Dish ranged between 10 to 20.

Time-lapse equipment

The microscope is a phase contrast Nikon Inverted Eclipse Ti2-U, controlled by Nikon NIS-Elements Advanced Research software version 5.30. The microscope is equipped with a Nikon 4X objective MRH20045, a Nikon 10X objective MRH20105, and a Nikon 20X objective MRH48250. The images we use to perform the data analysis are taken with the 20X objective, but we also use the 4X objective for some auxiliary tasks. The camera is a Nikon DS-Qi2 monochrome 14bit with a resolution of 16.25 megapixels. Within the microscope there is an Okolab (Pozzuoli, Italy) stagetop chamber incubator, H301-NIKON-TI-S-ER, equipped with a two-well base H101-2 X 35-M, designed to host two dishes. The chamber incubator is mounted on the motorized translational stage Nikon Ti2-S-SS-E. The gas mixture is controlled by an Okolab Bold-Line module H301-T-UNIT-BL-PLUS (Okolab-BL). Redundant measurements of temperature and CO_2 are performed with an Okolab-LEO module.

The time lapse sampling period of experiments 20230113 and 20230503 was 20 minutes, while the sampling period of experiments 20240627, 20240924, 20241017, 20241112, 20241203, 20250313 and 20250328 was 15 minutes. This change in the sampling period was due to the need to simplify and therefore speed up the tracking procedure.

Culture control during time-lapse

The conditions of the cell culture during time lapse were standard, namely: humidity = 90%, CO_2 = 5%, temperature = 37° C. *Gas control:* The gas mixture of air, water and CO_2 was produced and monitored by the Okolab-BL module; water to provide humidity was filtered and autoclaved. To have an independent control of the CO_2 concentration within the incubator, we measure and store it every 5 minutes through the Okolab-LEO module: gas is pumped out of the incubator into the LEO for 3 minutes, so that an independent reliable determination of the CO_2 concentration can be made. In the months before the experiment started, we calibrated this double-monitoring system in such a way to have consistent readings within the same incubator. *Temperature control:* The incubator hosts two dishes. The first dish is the one that we use for the time-lapse, seeded with BMSCs, in which there are no temperature probes, in order not to perturb, nor contaminate in any way the cells; the second dish, at a distance of 6 cm from the cell-seeded dish, is used exclusively for temperature control (the Temperature-Control Petri, T-CP). In the T-CP there is an amount of sterilized SIGMA water identical to the amount of medium in the cell-seeded dish (2 ml). Within the T-CP are located two temperature probes; the first one is used by the Okolab-BL module to fix the temperature at 37 degrees, through a digital feedback; the second probe is connected to the Okolab-LEO module that performs an independent measurement of the temperature every 5 minutes. In the months before the experiment started, we calibrated this double-monitoring system in the following way: we located the T-probe connected to the Okolab-BL module within the T-CP and the T-probe connected to the LEO within the dish that would contain the cells in a real experiment, and checked that the two readings were consistent with each other; during this testing period the discrepancy between the two temperature probes has always been lower than 0.2° C.

Selection of the originating cells

Six hours after the primary dish is seeded with cells, the dish is inserted into the microscope incubator. The first thing we need to do is to identify a couple of cells in the dish in order to tune the focus of the 4X objective; this procedure (which needs to be performed in live imaging) never takes more than 10 minutes, and often significantly less. When the focus of the 4X objective is fixed, we scan the entire dish; the scan is performed by taking $8 \times 8 = 64$ photos covering the entire dish. The image resulting from this scan is then used to select the originating cells to monitor during the experiment (see below). It is very important that this selection phase (which may be long, typically up to 1 hour) is not performed in live imaging with the microscope lamp on, because that would increase dramatically the danger of phototoxicity (see below). By working on the scan photograph, we can leave dark the cell-seeded dish. Nevertheless, it is advisable to keep the selection procedure as quick as possible to avoid that potentially isolated cells candidates start dividing before the time-lapse is initiated.

Within this study we only consider BMSC colonies that are derived from one single cell (single-cell-derived colonies, in the classification of [21]). Moreover, we only monitor colonies that are not infiltrated by other colonies during the time-lapse. To meet these two requirements we seed the Petri dish at very low densities (see above), in order to have a higher probability to find isolated originating cells. The fact that the initial cell must be isolated has a twofold importance: first, by selecting an isolated cell we give to the colony generated by that cell the necessary space to proliferate without interfering with other colonies during the time duration of the experiment; hence, here by 'isolated' we mean that the distance from another originating cell must be of the same order as (or larger than) the average size of the colonies at generation $k = 7$. Secondly, by selecting only isolated cells, we are sure to avoid cases in which we have two (or more) cells close to each other at the beginning of the experiment, because in that case we cannot be sure whether the nearby cells are sisters or not, which is essential to define single-cell-derived colonies. Given the very low seeding density, the size of our dish, and the size of the colonies at $k = 7$, the isolation criterion severely limits the number of colonies we manage to successfully select and follow during each experiments; this is the chief reason why our experimental campaign lasted for so long. We never selected more than 20 initiator cells, only a handful of which generate colonies that are finally included in the study (see below).

Once the cells have been selected from the scan image, we switch to the 20X objective and fine-tune the focus for each one of the selected cells, in order to optimise the sharpness of the images; moreover, in this phase we tune the position of each selected originating cell in order for it to be precisely at the centre of the field of view. This procedure is quick (max 10 minutes) and it needs to be done in live imaging, with the lamp on. Finally, after the focus of the 20X objective is set, we start the time lapse.

Monitoring the experiment

The time-lapse experiment is monitored every 6 hours for its whole duration according to the following check-list: the temperatures measured by the two probes within the T-CP must be consistent with each other and both equal to $37° \pm 0.5°$ C; the graph in the past 6 hours of the temperatures measured by the two probes within the T-CP must show no anomaly; the CO_2 measured by the BL module at the gas source and by the LEO module within the incubator must be consistent with each other and both equal to $5\% \pm 0.2\%$; the graph in the past 6 hours of the CO_2 measured by the same two modules must show no anomaly; all photos must be sharp and all cells must be

well in focus; colonies are checked for the need to expand the field of view (see below); colonies are checked for infiltration (see below); a rough count of all cells within each colony is performed. Every 24 hours a scan of the entire dish at 4X is performed, to have a global view of the development of all colonies in the dish.

Field of view expansion

The field of view (FOV) around each colony is composed by $n \times n$ photographs at 20X, acquired by translating the chamber incubator with the motorized stage and stiched together by the proprietary Nikon software NIS-Elements; at the beginning of the time lapse, when there is only the originating cell within the FOV, we set $n = 3$. As the colonies grow it becomes necessary to expand the FOV, hence $n = 3, 5, 7, \ldots$. We always use an odd value of n in such a way that the FOV before and after the expansion have the same center, which simplifies the subsequent image analysis. Our current version of the software does not allow to selectively expand the FOV of only certain colonies, therefore a FOV expansion from n to $n + 2$ implies a significant increase of the total number of photographs taken at each iteration of the time lapse; this puts some constraints related to phototoxicity that we discuss below.

Criteria to stop monitoring colonies

During the experiment we can stop monitoring a colony for one of the following reasons: **1.** Despite the isolation criterion, a colony may come in contact with another colony during the experiment (infiltration); in that case we stop monitoring and we discard it for data analysis. The infiltration criterion we use is the following: colonies A and B are mutually infiltrated if the distance between the two closest cells of A and B is equal to (or smaller than) the mean inter-cell distance within A and B. **2.** A selected originating cell may either die or detach from the dish before starting mitosis; in this case we stop monitoring it. **3.** When a selected originating cell does not make the first division within 4 days, we stop monitoring it. **4.** If one or more cells belonging to a colony drop out of the FOV before we manage to expand it, we stop monitoring that colony.

As a general rule, we keep monitoring all colonies that do not incur in the criteria above in order to avoid any selection bias. In some cases, though, it becomes necessary to forcibly reduce the number of colonies that we monitor with the time lapse. This happens because – as we have seen – as the colonies grow we need to expand the FOV; but as we shall see later on, the total number of photographs for each loop in the time-lapse is limited to 750, in order to avoid phototoxicity; hence, when FOV expansion is absolutely urgent, but we would exceed the total number of 750 photographs, and no colonies match the discard criteria above, we cut one colony randomly.

Finally, of all colonies monitored during the experiment, we only include in our analysis those that produce *at least* two cells at generation $k = 7$, lest the seventh generation criterion we have adopted to characterise the whole study becomes void.

Medium replacement

Medium is changed on a 3-4 days schedule (typically every Tuesday and Friday, with the experiment starting on Friday), for the whole duration of the experiment. Whenever the medium is changed in the cell-seeded dish, the sterile water is also changed in the T-CP, so to have always the same amount of fluid in the two dishes, which is essential to have a reliable temperature control.

Illumination parameters and phototoxicity

To obtain brilliant and sharp images (which simplify immensely the whole chain of analysis downstream) one would ideally illuminate the cells as much as possible during imaging. However, this is not advisable, due to the grave danger of phototoxicity. In order to select the illumination parameters (light intensity, filters, exposure time), it is therefore essential to keep into account the potential phototoxic effects of a prolonged exposure of cells to light.

Phototoxicity is a very dangerous effect, which acts in a twofold way: directly, by interfering in a negative way with the various cellular processes, among other things depressing proliferation and increasing the apoptosis rate [58–64]; and indirectly, by altering the properties of the culture medium [65]. Phototoxicity can severely bias the data and it must therefore be kept strictly under control. The issue of phototoxicity, though, is very complex: experimental tests are few and conducted on rather diverse cell types, by observing different cellular traits; hence, establishing a consensus in the literature on a danger threshold of the light level is difficult.

The chief parameter to assess the impact of phototoxicity is *fluence*, defined as the energy per unit area hitting the culture surface, measured in Joule per square centimetre (J/cm^2). In BMSCs, the reported critical value of fluence, above which clear effects on cellular processes are observed, ranges from 21 J/cm^2 [58], to 12 J/cm^2 [61], but the danger threshold has been estimated as low as 4 J/cm^2, in ASC cells [62]. Regarding medium degradation, the most recent experiments indicate a toxicity threshold of 21 J/cm^2 [65]. Given these results and given the lack of information about fluence and illumination parameters in most – if not all – time-lapse studies of BMSCs, we set the parameters in such a way to stay well below the lowest of the bounds mentioned above, namely that of 4 J/cm^2. To do that, we proceed as follows.

In all our experiments the light intensity of the LED lamp of the microscope (Cree, Inc. XM-L2 series, XLMBWT - 00-0000 - 0000T60E2) is reduced by 5 stops (i.e. by a factor $2^5 = 32$), by means of a neutral filter. By using a power meter (Thorlabs PM200, sensor Thorlabs S170C), we measured the power of the filtered light; even though the power does not depend on the objective, each objective requires a different phase filter to work, and the intensity of the light received by the sample *does* depend on the phase filter. Hence, all power measurements must be performed with the appropriate phase filter. To compute the power, the meter needs as an input the wavelength of the LED light; our LED's spectrum has two primary peaks at 440 nm and 540 nm; to be conservative in our estimates of the fluence we input in the power meter the wavelength of the most energetic peak (440 nm). The power is the energy per unit time (milliwatt, mW), hence by dividing the measured power by the area of the disc of light produced by the lamp (0.64 cm^2), we obtain the power per unit area that the sample receives, which is called *irradiance* (notice that for this to be true the light disc area must be smaller than the sensor area, which is the case in our measurement setup; otherwise the power must be divided by the sensor area); irradiance is measured in mW/cm^2. Once the irradiance is determined, the fluence – namely the total energy per unit area that the sample receives, J/cm^2 – is obtained by multiplying the irradiance by the exposure time. The exposure time depends on the specific phase of the experiments; these below are the values of the illumination parameters, and relative irradiance and fluence, during each one of the phases when the microscope lamp is on:

Initial cell search – Once the cell-seeded dish is inserted into the microscope incubator we first need to identify a couple of sample cells, in order to tune the focus on them. In this phase, the light intensity is set at 40%, the 5 stops filter is on, and we use a 4X objective, giving an irradiance of 0.0086 mW/cm^2; the camera sensor gain is

set at 1.0X. The search lasts a maximum of 10 minutes (often significantly less), giving a fluence smaller than 0.006 J/cm^2. This operation is done once in the experiment.

Scan of the Petri dish – We scan the cell-seeded dish at the beginning of the experiment in order use the scan to identify candidate cells; moreover, we scan every 24 hours the dish to have a global view. During this task, the light intensity is set at 4%, the 5 stops filter is on, and we use a 4X objective, giving an irradiance of 0.70 μW/cm^2; the camera sensor gain is set at 1.0X. The scan is performed by taking $8 \times 8 = 64$ photos, and the exposure time of each photo is 2 seconds, giving a fluence of 9.0×10^{-5} J/cm^2. This operation is done every 24 hours.

Focus fine-tuning – Once the originating cells are selected we fine-tune the focus for each cell. In this phase, the light intensity is set at 75%, the 5 stops filter is on, and we use a 20X objective, giving an irradiance of 1.0 mW/cm^2. The procedure lasts a maximum of 10 minutes, giving a fluence smaller than 0.6 J/cm^2; the camera sensor gain is set at 4.1X. This operation is done once in the experiment.

Time lapse – During the time-lapse the light intensity is set at 75%, the 5 stops filter is on, and we use a 20X objective, giving an irradiance of 1.0 mW/cm^2. The exposure time of each photo is 80 ms, corresponding therefore to a fluence-per-photo of 8×10^{-5} J/cm^2; the camera sensor gain is set at 4.1X. At each iteration of the loop, the system takes $n \times n$ photos around each colony, where $n = 3, 5, 7, 9, \ldots$. If we are following C colonies, the total number of photos at each loop iteration is n^2C; we always keep this total number below 750 (in the most flourishing experiments, we may have 6 colonies, each one covered by a 11×11 photo tiling, giving a total of 726 photos at each iteration). In this way we have a maximum fluence of $8 \times 10^{-5} \times 750 = 0.06$ J/cm^2 for each loop iteration. The whole loop repeats after 15 minutes. We therefore have a time-lapse fluence that is 66.6 times lower than the most conservative bound found in the literature (0.06 J/cm^2 vs 4.0 J/cm^2). Hence, we are rather confident that our observations of BMSCs have not been biased by phototoxicity.

During the preparation and for the entire duration of the time-lapse all lights in the lab are off, including all instruments lights and displays; windows and doors are shielded.

Control dish

When the cell-seeded dish for time-lapse microscopy is prepared, a second dish with identical procedure and seeding is also prepared and kept in a different (large) incubator (Heracell, Heraeus) as a control; this is the Control Dish (CD). The CD is not exposed to any light (besides the room and hood lights during medium changes), nor perturbation, and it undergoes medium replacements at identical times as the time-lapse dish. At the end of the experiment we perform a comparative analysis of the dish used for the time-lapse vs the CD, including a 4X scan of both of them. In this way we can be certain that there are no strong statistical differences between the two dishes, and therefore conclude that the culture conditions were identical, so that the time lapse experiment has not interfered in any way with the proliferation of the cells. This check is of great importance, especially in connection with the risk of phototoxicity: since this risk is negligible for the CD (which is kept in the dark), comparable proliferation rate and vitality of the two dishes is a further test that no phototoxic effects are in action. All experiments used in this study passed this test.

Cell tracking software

To work out the lineage of a colony it is necessary to determine the relationships between mother and daughter cells, and to work out precisely all division times. To do this a C/C++ program was developed, based on the OpenCV computer vision

library [66]. Each of the 28 colony was semi-manually tracked, requiring an average of 13 to 15 hours of work per colony. The tracking program has a graphical user interface consisting of two windows: the first displays the acquired images and the second shows the lineage tree that is progressively formed during the tracking process. Since all colonies are single-cell derived, the first step of the procedure is to tag the originating cell in the first frame of the acquisition by mouse-clicking on it; in that way the starting root link of the colony's lineage tree is generated. The originating cell is special in the lineage, because we have no information about the mitosis generating it; hence, no division time is associated to the originating cell. The next step is to connect the generating cell to its two daughter cells: the originating cell is selected in the lineage tree, which associate a label to that cell; the operator then scrolls through the sequence of images following the cell until reaching the images showing the initiation of the mitosis.

Identifying the mitosis

The precise determination of the division times is crucial for the analyses conducted in this study, hence it is essential to use a well-defined marker of mitosis to uniquely identify one precise moment during the mitosis phase of the cell cycle. Mitosis consists of several phases of different durations; the most distinctive and shortest phase is the mitotic cell rounding [67, 68], during which the cell assumes an almost spherical shape, appearing as a bright, circular object in the image (see Fig.1). This trait is easily recognisable in the image and it was chosen as marker of mitosis. The same criterion has been adopted in other studies [21]. Clicking on the image corresponding to the mitotic rounding sets the stopping time of the mother cell and the starting time of the two daughter cells; these time-stamps are later used to determine the division time τ of each cell. At the frame corresponding to the mitotic rounding the two daughter cells are still not distinguishable from each other, hence the operator scrolls on through the sequence of images until the nuclei of the two daughters are clearly separated; at that point the operator clicks on the two daughters, thus assigning a new label to each one of them; these labels are connected to the mother's label by the corresponding mitosis. The process is repeated recursively for all cells, until the seventh generation is reached. Cells of the seventh generation are no longer followed, so they only have the starting time, hence we do not have the division times of the cells of generation $k = 7$.

One may ask why we use the cell rounding as marker of mitosis, instead of simply using the same frame as we use to label to two daughters. The answer is that deciding what is the first image at which the two daughters' nuclei are clearly separated from each other has a large degree of arbitrariness and it is operator-dependent; therefore, it is not advisable to use this frame as a marker of mitosis (for safety, we anyway checked that these two times are perfectly correlated to each other - see Fig.S5). On the other hand, the arbitrariness in the selection of the first image in which the two daughters are well-separated has no consequences on any observable, as it is only used to assign a label to the two daughters.

Criterion for G_0 phase

During tracking, two special cases can occur: 1) A cell commits apoptosis and dies; this process is very clear in the imaging, hence there is no ambiguity in its identification; the cell is tagged as 'dead' in the lineage tree and graphically indicated with a red dot. 2) A cell stops dividing, going into the G_0 phase. We have defined a G_0 cell as a cell that has not divided for a period of 84 hours since its birth. For further details on the robustness of this criterion see the main text. Such cells are then

tagged as 'G_0' in the lineage tree and graphically indicated with a short black transverse segment (or cap).

Determination of the P-value

To assess the significance of correlation between two sets of variables, $\{x_i\}$ and $\{y_i\}$, we proceed as follows. First, we calculate the Spearman correlation coefficient ρ on the actual experimental variables. Then, we randomly scramble the positions of the values in the first set, $\{x_i\}$, hence cutting all possible correlations between the two variables, and we recalculate ρ; we repeat the random scrambling 10^6 times, and calculate the fraction of cases that give a correlation coefficient ρ larger than or equal to the experimental one. This fraction is the P-value of Spearman correlation; notice that with this procedure the most significant signal that we can get has P-value $< 10^{-6}$. The P-value defined in this way is therefore equal to the probability that the correlation found in the data is accidentally present also in an uncorrelated random dataset of the same size and of the same nature as the experimental one. The procedure we use to assign a P-value to the inheritance test is analogous: we randomly scramble the experimental lineage tree 10^6 times, and calculate the fraction of scrambled trees with entropy smaller than or equal to the experimental one.

Funding

This work was supported by the following grants: ERC Advanced Grant RG.BIO (Contract No. 785932) to ACa; MIUR Grant INFO.BIO (Protocol No. R18JNYYMEY) to ACa; MIUR Grant PRIN2020 (Contract No. 2020PFCXPE-005) to IG; Grant SIOMMMS - Premi di Ricerca 2022 to BP.

Acknowledgments

It is a pleasure to acknowledge several inspiring discussions with the late Paolo Bianco and with Giorgio Parisi during the very early stages of this project. We thank Pietro Cirigliano, Roberto Di Leonardo, Francis Allen Farrelly, Giacomo Frangipane, Emiliano Lalli, Federica Massa and Shoichi Yip for technical help. ACa and TSG thank Enzo Branchini for discussions within the CC. ACa acknowledges the support and the advice of the late Giovanni Cavagna.

Author Contributions - CRediT Taxonomy

· Alessandro Allegrezza - Roles: Data curation.
· Riccardo Beschi - Roles: Investigation, Data Curation.
· Domenico Caudo - Roles: Investigation, Data Curation.
· Andrea Cavagna - Roles: Conceptualization, Investigation, Data Curation, Formal Analysis, Funding Acquisition, Methodology, Project Administration, Supervision, Validation, Writing - Original Draft Preparation, Writing - Review & Editing.
· Alessandro Corsi - Roles: Resources, Writing - Review & Editing.
· Antonio Culla - Roles: Investigation, Data Curation.
· Samantha Donsante - Roles: Resources, Data Curation.
· Giuseppe Giannicola - Roles: Resources.
· Irene Giardina - Roles: Conceptualization, Data Curation, Formal Analysis, Funding Acquisition, Resources, Writing - Original Draft Preparation, Writing - Review & Editing.

· Giorgio Gosti - Roles: Methodology, Validation.
· Tomas S. Grigera - Roles: Conceptualization, Formal Analysis, Methodology, Software, Writing - Original Draft Preparation, Writing - Review & Editing.
· Stefania Melillo - Roles: Conceptualization, Formal Analysis, Investigation, Data Curation, Methodology, Validation, Visualization.
· Biagio Palmisano - Roles: Investigation, Resources, Validation, Data curation, Writing - Review & Editing.
· Leonardo Parisi - Roles: Formal Analysis, Investigation, Data Curation, Methodology, Software, Validation, Visualization.
· Lorena Postiglione - Roles: Methodology, Validation.
· Mara Riminucci - Roles: Resources, Writing - Original Draft Preparation, Writing - Review & Editing.
· Francesco Saverio Rotondi - Roles: Data Curation, Formal Analysis, Investigation, Software, Visualization.

References

1. Friedenstein A, Piatetzky-Shapiro I, Petrakova K. Osteogenesis in transplants of bone marrow cells. Development. 1966;16(3):381–390.

2. Friedenstein AJ, Chailakhyan RK, Latsinik NV, Panasyuk AF, Keiliss-Borok IV. Stromal cells responsible for transferring the microenvironment of the hemopoietic tissues: cloning in vitro and retransplantation in vivo. Transplantation. 1974;17(4):331–340.

3. Owen M, Friedenstein A. Stromal stem cells: Marrow-derived osteogenic precursors. In: Ciba Foundation Symposium 136-Cell and Molecular Biology of Vertebrate Hard Tissues: Cell and Molecular Biology of Vertebrate Hard Tissues: Ciba Foundation Symposium 136. Wiley Online Library; 2007. p. 42–60.

4. Kuznetsov SA, Krebsbach PH, Satomura K, Kerr J, Riminucci M, Benayahu D, et al. Single-colony derived strains of human marrow stromal fibroblasts form bone after transplantation in vivo. Journal of bone and mineral research. 1997;12(9):1335–1347.

5. Donsante S, Palmisano B, Serafini M, Robey PG, Corsi A, Riminucci M. From stem cells to bone-forming cells. International journal of molecular sciences. 2021;22(8):3989.

6. Sacchetti B, Funari A, Michienzi S, Di Cesare S, Piersanti S, Saggio I, et al. Self-renewing osteoprogenitors in bone marrow sinusoids can organize a hematopoietic microenvironment. Cell. 2007;131(2):324–336.

7. Tormin A, Li O, Brune JC, Walsh S, Schütz B, Ehinger M, et al. CD146 expression on primary nonhematopoietic bone marrow stem cells is correlated with in situ localization. Blood, The Journal of the American Society of Hematology. 2011;117(19):5067–5077.

8. Rennerfeldt DA, Van Vliet KJ. Concise review: when colonies are not clones: evidence and implications of intracolony heterogeneity in mesenchymal stem cells. Stem cells. 2016;34(5):1135–1141.

9. Satomura K, Derubeis AR, Fedarko NS, Ibaraki-O'Connor K, Kuznetsov SA, Rowe DW, et al. Receptor tyrosine kinase expression in human bone marrow stromal cells. Journal of Cellular Physiology. 1998;177(3):426–438.

10. Sworder BJ, Yoshizawa S, Mishra PJ, Cherman N, Kuznetsov SA, Merlino G, et al. Molecular profile of clonal strains of human skeletal stem/progenitor cells with different potencies. Stem Cell Research. 2015;14(3):297–306.

11. James S, Fox J, Afsari F, Lee J, Clough S, Knight C, et al. Multiparameter analysis of human bone marrow stromal cells identifies distinct immunomodulatory and differentiation-competent subtypes. Stem cell reports. 2015;4(6):1004–1015.

12. Schroeder T. Long-term single-cell imaging of mammalian stem cells. Nature methods. 2011;8(4):S30–S35.

13. Hilsenbeck O, Schwarzfischer M, Skylaki S, Schauberger B, Hoppe PS, Loeffler D, et al. Software tools for single-cell tracking and quantification of cellular and molecular properties. Nature biotechnology. 2016;34(7):703–706.

14. Shen Q, Wang Y, Dimos JT, Fasano CA, Phoenix TN, Lemischka IR, et al. The timing of cortical neurogenesis is encoded within lineages of individual progenitor cells. Nature neuroscience. 2006;9(6):743–751.

15. Eilken HM, Nishikawa SI, Schroeder T. Continuous single-cell imaging of blood generation from haemogenic endothelium. Nature. 2009;457(7231):896–900.

16. Ravin R, Hoeppner DJ, Munno DM, Carmel L, Sullivan J, Levitt DL, et al. Potency and fate specification in CNS stem cell populations in vitro. Cell stem cell. 2008;3(6):670–680.

17. Plambeck M, Kazeroonian A, Loeffler D, Kretschmer L, Salinno C, Schroeder T, et al. Heritable changes in division speed accompany the diversification of single T cell fate. Proceedings of the National Academy of Sciences. 2022;119(9):e2116260119.

18. Seiler C, Gazdhar A, Reyes M, Benneker LM, Geiser T, Siebenrock KA, et al. Time-lapse microscopy and classification of 2D human mesenchymal stem cells based on cell shape picks up myogenic from osteogenic and adipogenic differentiation. Journal of tissue engineering and regenerative medicine. 2014;8(9):737–746.

19. Whitfield MJ, Lee WCJ, Van Vliet KJ. Onset of heterogeneity in culture-expanded bone marrow stromal cells. Stem Cell Research. 2013;11(3):1365–1377.

20. Lee WC, Shi H, Poon Z, Nyan LM, Kaushik T, Shivashankar G, et al. Multivariate biophysical markers predictive of mesenchymal stromal cell multipotency. Proceedings of the National Academy of Sciences. 2014;111(42):E4409–E4418.

21. Rennerfeldt DA, Raminhos JS, Leff SM, Manning P, Van Vliet KJ. Emergent heterogeneity in putative mesenchymal stem cell colonies: Single-cell time lapsed analysis. PLoS One. 2019;14(4):e0213452.

22. Powell E. Some features of the generation times of individual bacteria. Biometrika. 1955;42(1/2):16–44.

23. Nachtwey D, Cameron I. Cell cycle analysis. In: Methods in Cell Biology. vol. 3. Elsevier; 1969. p. 213–259.

24. Cheung TH, Rando TA. Molecular regulation of stem cell quiescence. Nature reviews Molecular cell biology. 2013;14(6):329–340.

25. Mens MM, Ghanbari M. Cell cycle regulation of stem cells by microRNAs. Stem cell reviews and reports. 2018;14:309–322.

26. Stenderup K, Justesen J, Clausen C, Kassem M. Aging is associated with decreased maximal life span and accelerated senescence of bone marrow stromal cells. Bone. 2003;33(6):919–926.

27. Wagner W, Horn P, Castoldi M, Diehlmann A, Bork S, Saffrich R, et al. Replicative senescence of mesenchymal stem cells: a continuous and organized process. PloS one. 2008;3(5):e2213.

28. He L, Li M, Wang X, Wu X, Yue G, Wang T, et al. Morphology-based deep learning enables accurate detection of senescence in mesenchymal stem cell cultures. BMC biology. 2024;22(1):1.

29. Hormoz S, Desprat N, Shraiman BI. Inferring epigenetic dynamics from kin correlations. Proceedings of the National Academy of Sciences. 2015;112(18):E2281–E2289.

30. Hicks DG, Speed TP, Yassin M, Russell SM. Maps of variability in cell lineage trees. PLoS computational biology. 2019;15(2):e1006745.

31. Harris TE, et al. The theory of branching processes. vol. 6. Springer Berlin; 1963.

32. Haccou P, Jagers P, Vatutin VA. Branching processes: variation, growth, and extinction of populations. 5. Cambridge university press; 2005.

33. Smith J, Martin L. Do cells cycle? Proceedings of the National Academy of Sciences. 1973;70(4):1263–1267.

34. Weber TS, Jaehnert I, Schichor C, Or-Guil M, Carneiro J. Quantifying the length and variance of the eukaryotic cell cycle phases by a stochastic model and dual nucleoside pulse labelling. PLoS computational biology. 2014;10(7):e1003616.

35. Lavalle NG, Chara O, Grigera TS. Fluctuations in tissue growth portray homeostasis as a critical state and long-time non-Markovian cell proliferation as Markovian. Royal Society Open Science. 2023;10(9):230871.

36. Yates CA, Ford MJ, Mort RL. A multi-stage representation of cell proliferation as a Markov process. Bulletin of mathematical biology. 2017;79:2905–2928.

37. Liu L, Michowski W, Kolodziejczyk A, Sicinski P. The cell cycle in stem cell proliferation, pluripotency and differentiation. Nature cell biology. 2019;21(9):1060–1067.

38. Pauklin S, Vallier L. The cell-cycle state of stem cells determines cell fate propensity. Cell. 2013;155(1):135–147.

39. Dalton S. Linking the cell cycle to cell fate decisions. Trends in cell biology. 2015;25(10):592–600.

40. Mareddy S, Crawford R, Brooke G, Xiao Y. Clonal isolation and characterization of bone marrow stromal cells from patients with osteoarthritis. Tissue engineering. 2007;13(4):819–829.

41. Mareddy S, Dhaliwal N, Crawford R, Xiao Y. Stem Cell–Related Gene Expression in Clonal Populations of Mesenchymal Stromal Cells from Bone Marrow. Tissue Engineering Part A. 2010;16(2):749–758.

42. Ahn EY, Lim ST, Cook WJ, McDonald JM. Calmodulin binding to the Fas death domain: regulation by Fas activation. Journal of Biological Chemistry. 2004;279(7):5661–5666.

43. Colless DH. Phylogenetics: the theory and practice of phylogenetic systematics; 1982.

44. Fischer M, Herbst L, Kersting S, Kühn AL, Wicke K. Tree balance indices: A comprehensive survey. Springer Nature; 2023.

45. Theil H. Economics and information theory. Amsterdam: North-Holland,; 1967.

46. Chang HH, Hemberg M, Barahona M, Ingber DE, Huang S. Transcriptome-wide noise controls lineage choice in mammalian progenitor cells. Nature. 2008;453(7194):544–547.

47. Ng RK, Gurdon JB. Epigenetic inheritance of cell differentiation status. Cell cycle. 2008;7(9):1173–1177.

48. Zion EH, Chandrasekhara C, Chen X. Asymmetric inheritance of epigenetic states in asymmetrically dividing stem cells. Current opinion in cell biology. 2020;67:27–36.

49. Sandler O, Mizrahi SP, Weiss N, Agam O, Simon I, Balaban NQ. Lineage correlations of single cell division time as a probe of cell-cycle dynamics. Nature. 2015;519(7544):468–471.

50. Mosheiff N, Martins BM, Pearl-Mizrahi S, Grünberger A, Helfrich S, Mihalcescu I, et al. Inheritance of cell-cycle duration in the presence of periodic forcing. Physical Review X. 2018;8(2):021035.

51. Hormoz S, Singer ZS, Linton JM, Antebi YE, Shraiman BI, Elowitz MB. Inferring cell-state transition dynamics from lineage trees and endpoint single-cell measurements. Cell systems. 2016;3(5):419–433.

52. Wagner DE, Klein AM. Lineage tracing meets single-cell omics: opportunities and challenges. Nature Reviews Genetics. 2020;21(7):410–427.

53. Baron CS, van Oudenaarden A. Unravelling cellular relationships during development and regeneration using genetic lineage tracing. Nature reviews molecular cell biology. 2019;20(12):753–765.

54. Weinreb C, Rodriguez-Fraticelli A, Camargo FD, Klein AM. Lineage tracing on transcriptional landscapes links state to fate during differentiation. Science. 2020;367(6479):eaaw3381.

55. Raj B. Single-Cell Profiling of Lineages and Cell Types in the Vertebrate Brain. In: Lineage Tracing: Methods and Protocols. Springer; 2025. p. 299–310.

56. Spanjaard B, Hu B, Mitic N, Olivares-Chauvet P, Janjuha S, Ninov N, et al. Simultaneous lineage tracing and cell-type identification using CRISPR–Cas9-induced genetic scars. Nature biotechnology. 2018;36(5):469–473.

57. Ihry RJ, Worringer KA, Salick MR, Frias E, Ho D, Theriault K, et al. p53 inhibits CRISPR–Cas9 engineering in human pluripotent stem cells. Nature medicine. 2018;24(7):939–946.

58. Surovtseva M, Surovtsev N, Bondarenko NA, Kim I, Lykov A, Poveshchenko O. Survival and Proliferation of Bone Marrow Derived Mesenchymal Stem Cells Under 532 nm Laser Irradiation. In: 2021 IEEE Ural-Siberian Conference on Computational Technologies in Cognitive Science, Genomics and Biomedicine (CSGB). IEEE; 2021. p. 160–163.

59. Laissue PP, Alghamdi RA, Tomancak P, Reynaud EG, Shroff H. Assessing phototoxicity in live fluorescence imaging. Nature methods. 2017;14(7):657–661.

60. Ong WK, Chen HF, Tsai CT, Fu YJ, Wong YS, Yen DJ, et al. The activation of directional stem cell motility by green light-emitting diode irradiation. Biomaterials. 2013;34(8):1911–1920.

61. Yuan Y, Yan G, Gong R, Zhang L, Liu T, Feng C, et al. Effects of blue light emitting diode irradiation on the proliferation, apoptosis and differentiation of bone marrow-derived mesenchymal stem cells. Cellular Physiology and Biochemistry. 2017;43(1):237–246.

62. Wang Y, Huang YY, Wang Y, Lyu P, Hamblin MR. Red (660 nm) or near-infrared (810 nm) photobiomodulation stimulates, while blue (415 nm), green (540 nm) light inhibits proliferation in human adipose-derived stem cells. Scientific reports. 2017;7(1):7781.

63. Tani A, Chellini F, Giannelli M, Nosi D, Zecchi-Orlandini S, Sassoli C. Red (635 nm), near-infrared (808 nm) and violet-blue (405 nm) photobiomodulation potentiality on human osteoblasts and mesenchymal stromal cells: a morphological and molecular in vitro study. International journal of molecular sciences. 2018;19(7):1946.

64. Li H, Wang S, Hui Y, Ren Y, Li J, Lan X, et al. The implication of blue light-emitting diode on mesenchymal stem cells: a systematic review. Lasers in Medical Science. 2023;38(1):267.

65. Magni G, Banchelli M, Ciaccheri L, Mazzoni M, Adinolfi B, Cavigli L, et al. Can photobiomodulation be studied in vitro? Investigation on the interaction between cell culture medium and short-wavelength blue LED light. In: Optical Interactions with Tissue and Cells XXXV. vol. 12840. SPIE; 2024. p. 92–96.

66. Bradski G. The opencv library. Dr Dobb's Journal: Software Tools for the Professional Programmer. 2000;25(11):120–123.

67. Taubenberger AV, Baum B, Matthews HK. The mechanics of mitotic cell rounding. Frontiers in cell and developmental biology. 2020;8:687.

68. Thery M, Bornens M. Get round and stiff for mitosis. HFSP Journal. 2008;2(2):65–71.

Supporting Information

Table S1

experiment [1]	DT (min) [2]	donor [3]	age [4]	sex [5]	passage [6]	colony [7]	N_G0 [8]	N_dead [9]	N_inactive [10]	N_miss [11]	mean tau (hours) [12]	gamma (1/hours) [13]	tau_min (hours) [14]	P_G0 [15]	P-value inheritance [16]
20230113	20	5	35	M	0	01	6	0	6	12	14.83	0.302	11.29	2.9E-10	6.84E-03
						07	0	0	0	0	12.97	0.527	11.20	2.2E-17	ND
						08	6	1	7	16	19.54	0.242	14.68	5.2E-08	7.52E-02
						09	14	0	14	100	19.87	0.189	14.12	1.8E-06	9.38E-03
20230503	20	6	32	M	0	13	11	0	11	24	19.78	0.205	14.25	6.2E-07	7.00E-06
						16	12	2	14	60	23.15	0.138	14.92	7.2E-05	8.10E-05
20240627	15	7	65	F	2	03	12	0	12	32	20.44	0.122	11.71	1.5E-04	1.20E-05
						04	18	4	22	120	26.16	0.055	8.41	1.6E-02	5.34E-03
						06	22	0	22	120	35.45	0.04	12.48	5.7E-02	1.26E-01
20240924	15	7	65	F	1	05	22	0	22	102	21.40	0.104	11.98	5.6E-04	4.50E-05
						12	23	0	23	76	21.20	0.096	10.60	8.7E-04	4.44E-02
20241017	15	10	62	F	1	02	0	0	0	0	14.74	0.538	13.14	2.8E-17	ND
						05	17	3	20	80	20.61	0.127	10.93	9.3E-05	1.70E-05
						09	12	1	13	90	18.52	0.158	11.62	1.1E-05	4.10E-05
						11	10	0	10	26	21.00	0.128	12.06	1.0E-04	1.98E-04
						16	2	1	3	8	17.62	0.209	12.33	3.1E-07	1.00E+00
20241112	15	10	62	F	1	02	1	1	2	4	19.18	0.213	14.29	3.6E-07	1.00E+00
						05	1	0	1	4	15.82	0.328	12.73	7.0E-11	ND
20241203	15	10	62	F	1	03	6	0	6	60	18.67	0.202	13.93	7.1E-07	8.20E-05
						07	22	2	24	100	24.92	0.061	8.47	1.0E-02	7.35E-03
						09	5	0	5	22	20.19	0.117	11.00	2.0E-04	9.28E-02
20250313	15	9	45	M	2	03	0	0	0	0	18.33	0.167	12.32	6.3E-06	ND
						14	16	0	16	100	21.06	0.115	11.45	2.4E-04	6.88E-04
20250328	15	12	43	F	1	02	3	0	3	12	19.60	0.18	13.85	3.3E-06	2.41E-01
						06	0	2	2	8	18.17	0.331	15.39	1.4E-10	3.19E-02
						11	6	0	6	12	24.29	0.111	14.94	4.7E-04	2.31E-04
						12	19	0	19	96	24.88	0.095	13.73	1.3E-03	2.77E-04
						16	2	0	2	6	17.89	0.235	13.77	6.8E-08	1.00E+00

Fig 6. Table S1. Detailed parameters of all colonies. [1] Date of the experiment; [2] time interval between frames in the time lapse; [3] donor's label; [4] donor's age; [5] donor's sex; [6] passage; [7] label of the colony within that experiment; [8] number of G_0 cells, N_{G_0}; [9] number of dead cells, N_{dead}; [10] number of inactive cells, $N_{\text{inactive}} = N_{G_0} + N_{\text{dead}}$; [11] number of missing cells at generation $k = 7$, N_{missing}; [12] mean division time of the colony, $\bar{\tau}$; [13] proliferation rate, γ, obtained from the gapped exponential fit; [14] minimum division time, $\tau_{\min}$, obtained from the gapped exponential fit; [15] probability of emergence of G_0 cells, p_{G_0}, under the (wrong) hypothesis that a G_0 cell is merely a cell with division time larger than 84 hrs, given by Eq.(3) in the main text; the actual number of G_0 cells in each colony is far larger than $128 \times p_{G_0}$, indicating that the tautological argument is wrong (see main text); [16] P-value of the inheritance test (strong significance - light green: P$<$ 0.01; fair significance - dark green: P$<$ 0.05; not significant - red: P $>$ 0.05; ND: Not Defined - grey (when the colony has 0 or 1 inactive cells the inheritance test cannot be run).

Figure S1

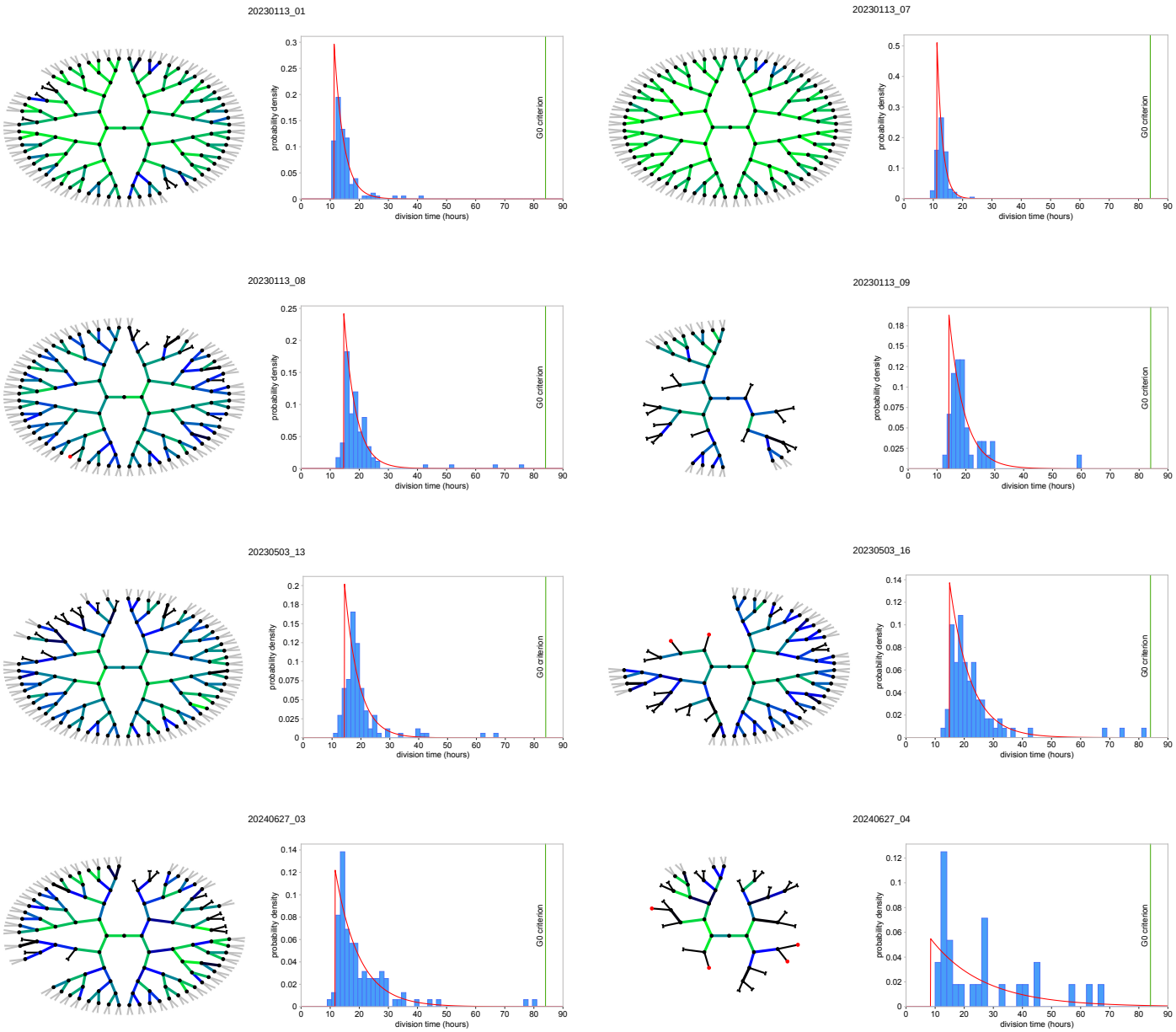

Fig S1. Lineage trees and division times histograms of all colonies. Abstract representation of the lineages of all the BMSC colonies in our dataset, including those reported in Fig.2. For each colony we also report the corresponding normalised histogram of the cells' division times, analogous to the ones in Fig.3.

Figure S1 (continued)

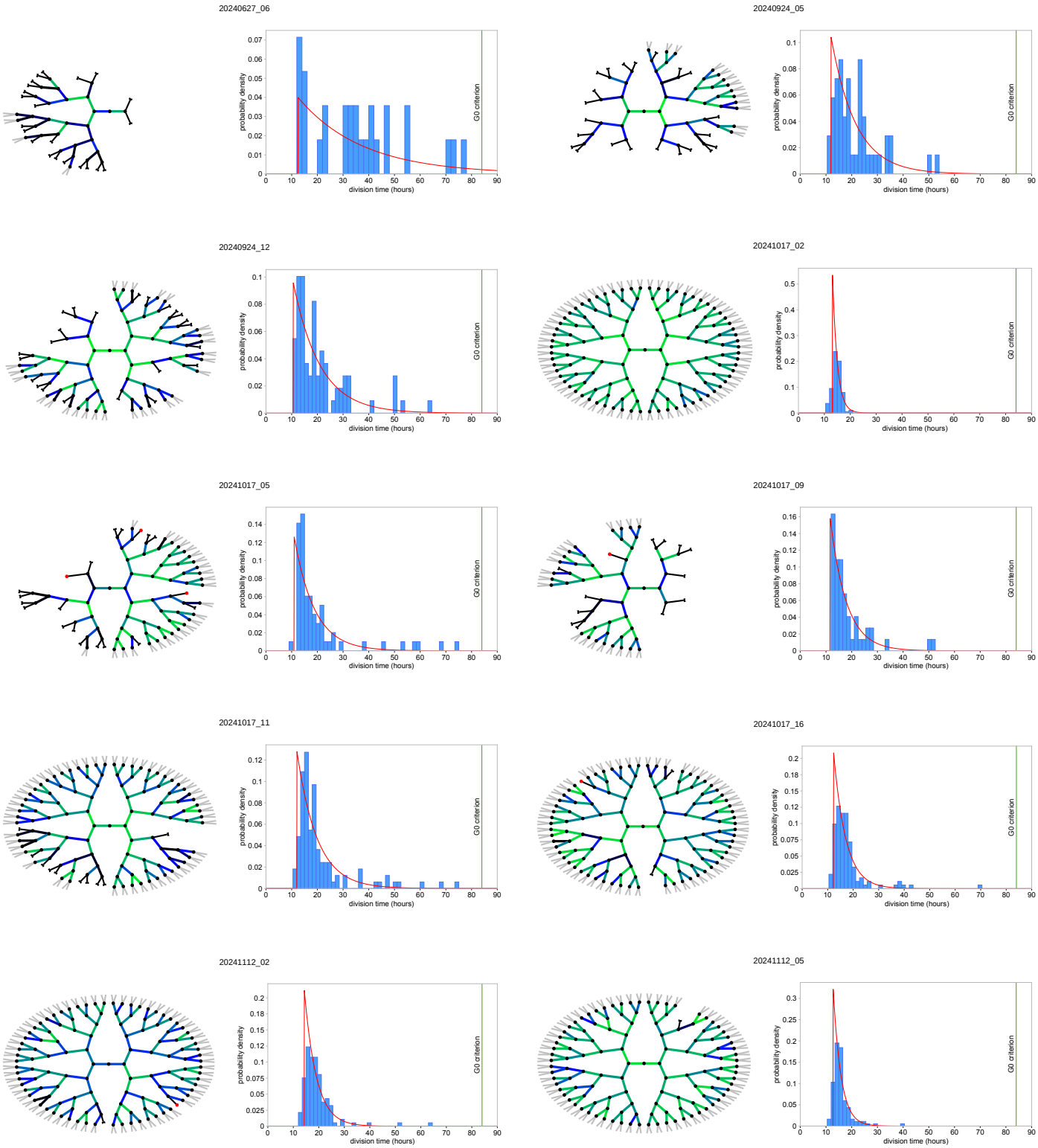

Figure S1 (continued)

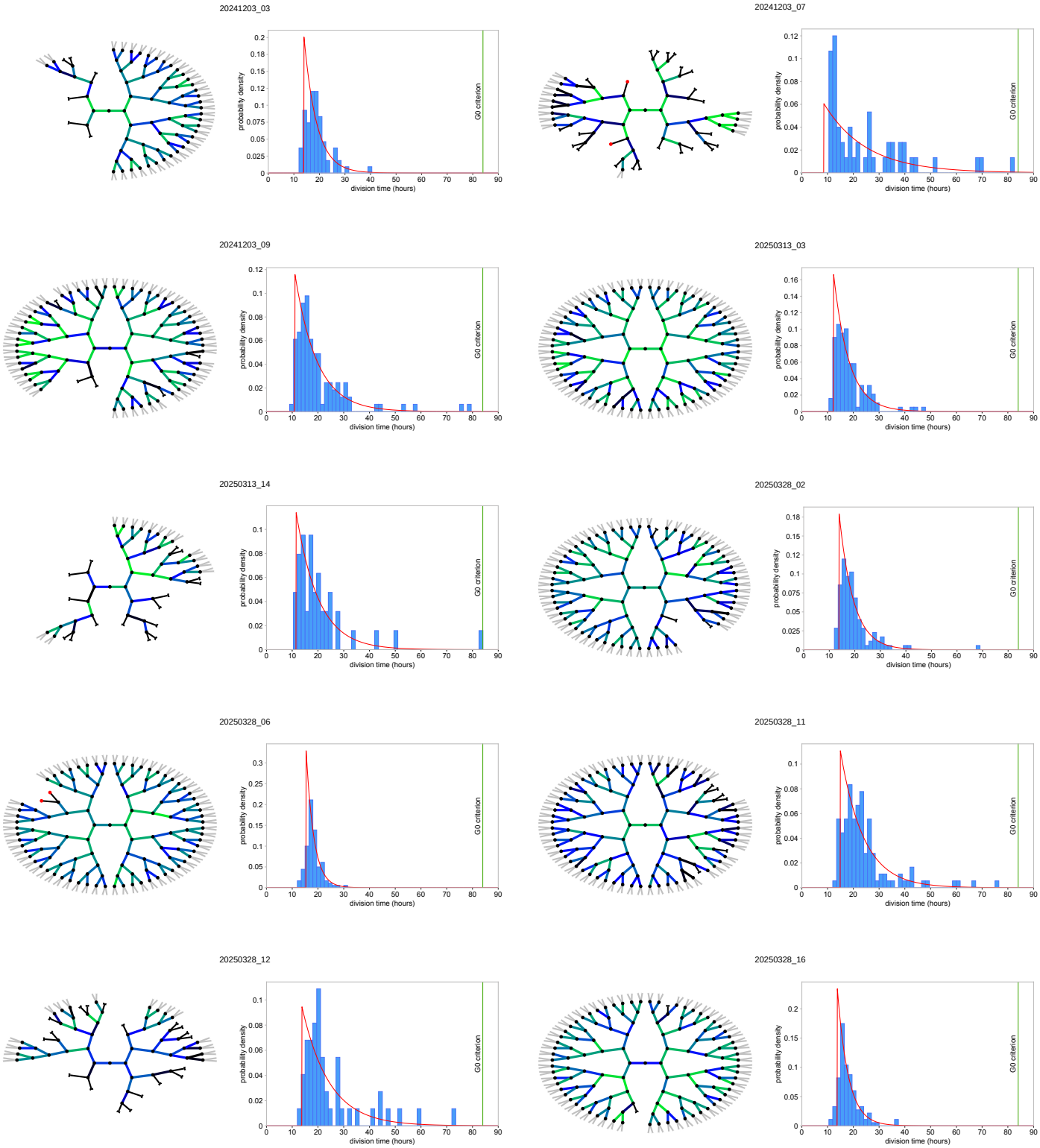

Figure S2

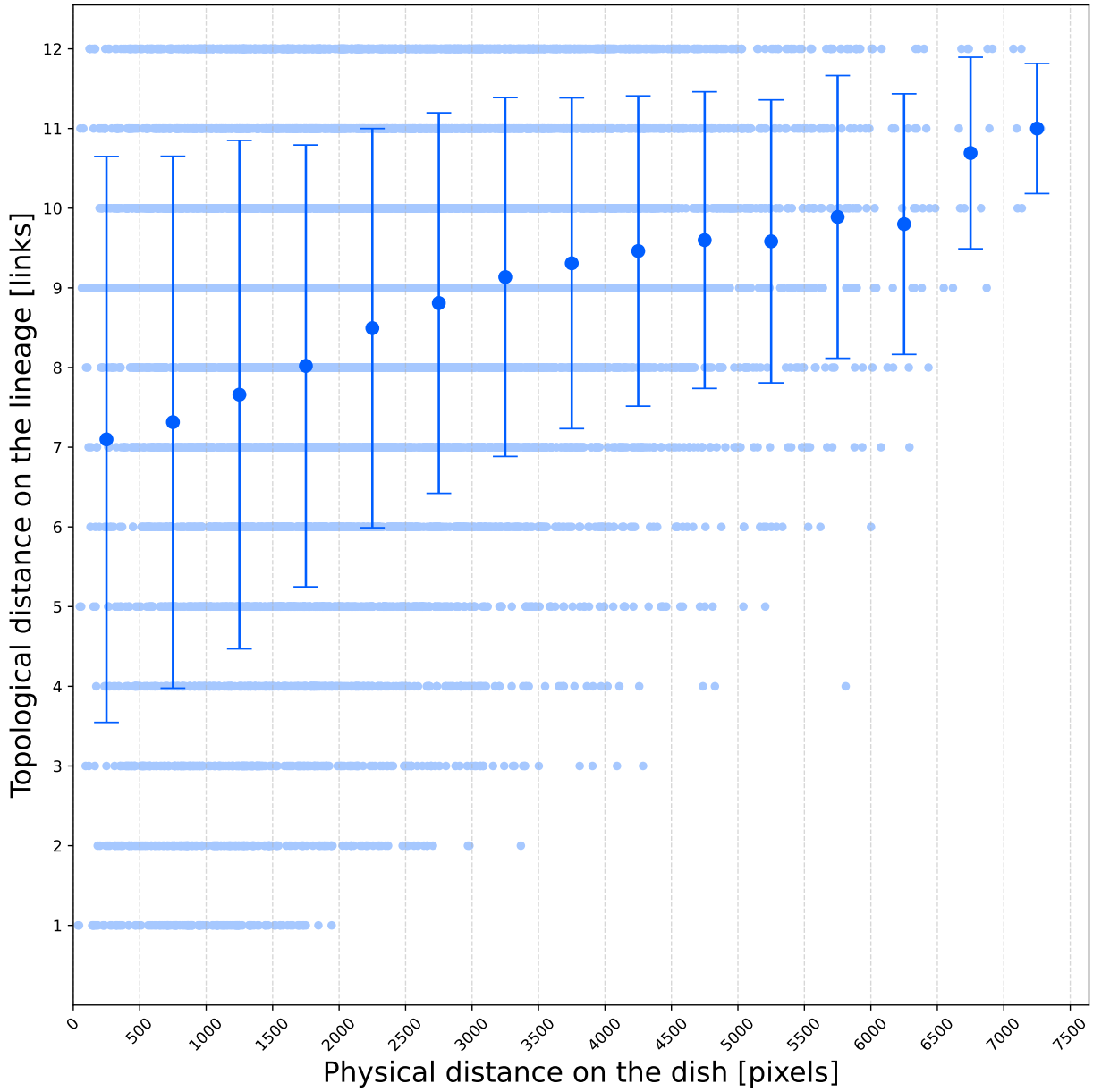

Fig S2. Distance on the tree vs distance on the dish. As a probe of the general relationship between topological distance on the tree and physical distance on the dish, we report here the mutual distances between all mitosis in a sample colony, 20241017-02 (light blue points); topological distance on the tree is measured in number of links separating two mitosis/nodes, while physical distance on the dish is measured in pixels separating the two mitosis. Correlation between the two types of distance is weak, with Spearman correlation coefficient $\rho = 0.24$ (P-value $< 10^{-6}$). Even small physical distances correspond to a very wide range of topological distances; this is clear if we group together all physical distances in bins of 500 pixels and average in each bin the relative topological distances (dark large points – error bars are standard deviations). This plot demonstrates that short topological distances correspond to short physical distances, but that short physical distances do not correspond to short topological distances. In other words, a small spot on the dish is mapped onto a very large"spot" on the tree; hence, spatial correlations are very unlikely to be the cause of the G_0 clustering that we find in the biological lineages.

Figure S3

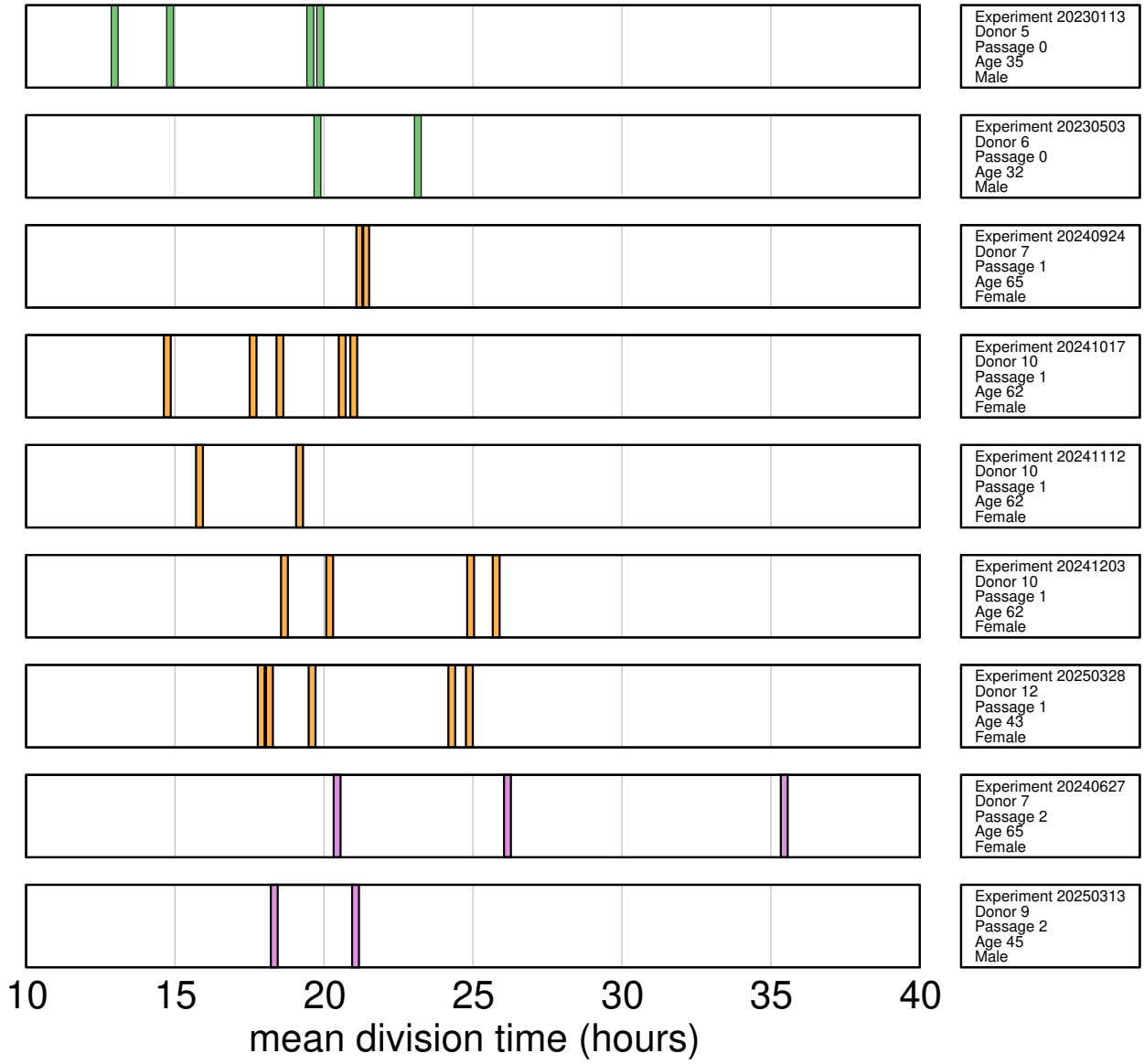

Fig S3. Variability with experiment, donor, age, sex, and passage. We report here the mean division time for each colony in the dataset, ordered according to experiment, donor, age, sex, and the passage of the cell culture. Each vertical bar corresponds to a different colony; colour represents passage: P0-green, P1-orange, P2-pink. Fluctuations within the same experiment are of the same order as the variability across the whole dataset. The only very weak correlation in the data is between division time and passage, although even that is borderline not-significant (Spearman correlation $\rho = 0.33$, P-value $= 0.09$). We notice that the only colony that seems an outlier in this plot is 20240627-06 (largest division time of experiment 20240627); interestingly, this is also the colony that seems anomalous in its inheritance test, as it yields a negative result with a large number of G_0 cells, and it is the only colony somehow detached from the bulk of points in the topology vs kinetics plot (see Fig.4).

Figure S4

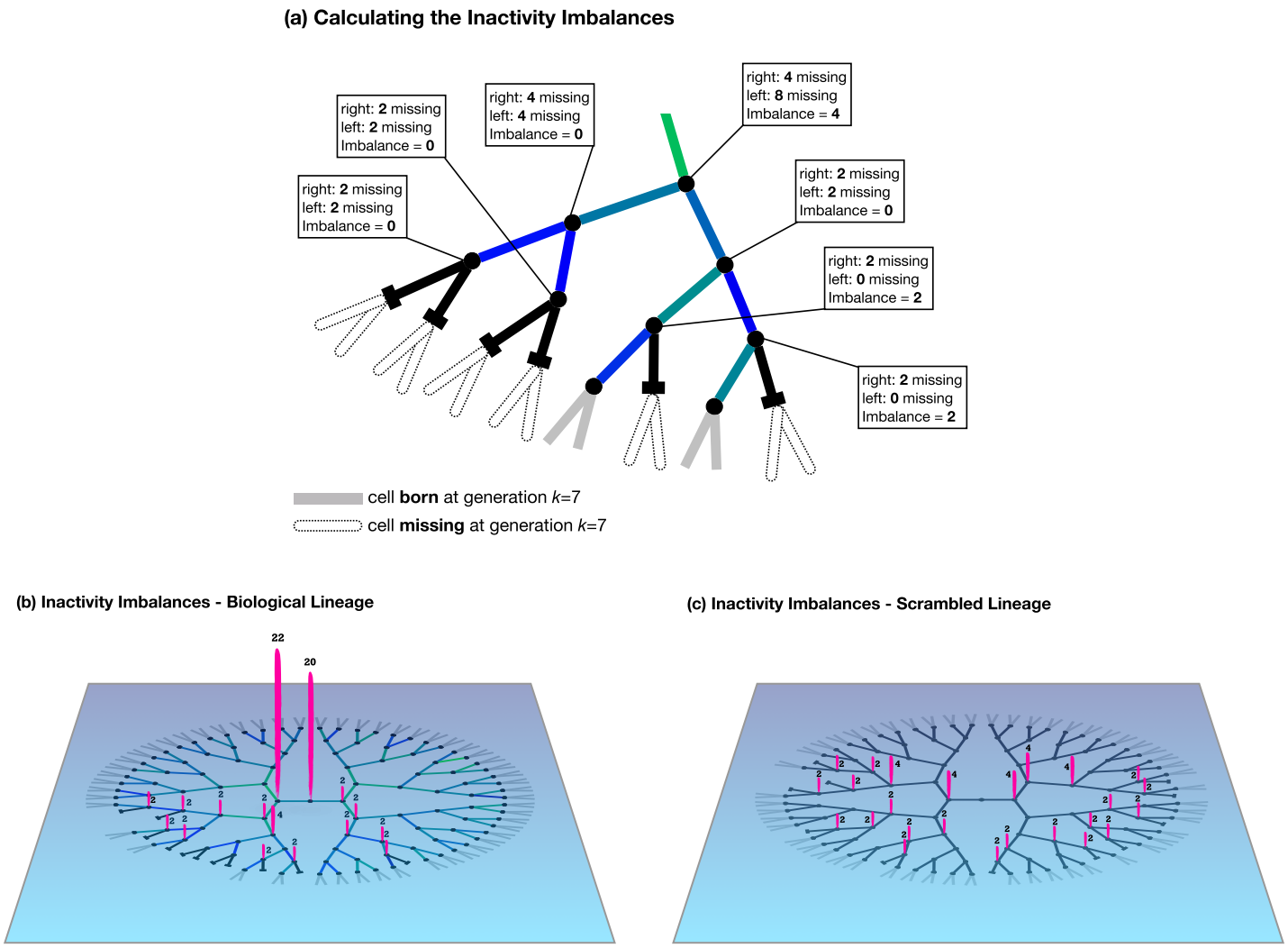

Fig S4. Inactivity Imbalances and Entropy. (a) We illustrate in this panel how the inactivity imbalances are calculated, using as an example a portion of real lineage, from colony 20230503-13. For each mitosis, or node, the inactivity imbalance is defined as the modulus of the difference between right and left sub-branches of the number of missing cells at generation $k = 7$ (dotted segments). **(b)** For lineage 20230503-13, the inactivity imbalance, I_m, is graphically represented as a purple vertical brushstroke on each mitosis, m (imbalances equal to zero are not marked). In this lineage most of the imbalance is concentrated on just two nodes (with imbalance 22 and 24); these two mitosis are those where it is more likely that there has been a change in the probability of emergence of inactive cells; on one other node the imbalance is 4, and on 13 nodes the imbalance is 2; in all other nodes the imbalance is zero. This large inequality of the imbalances across the lineage is the clearest symptom of inheritance. The entropy S measures exactly this inequality: it is a collective function of all non-zero imbalances, given by the formula, $S = -\sum_m (I_m/I_{\text{total}}) \log (I_m/I_{\text{total}})$, where the total imbalance is the sum of the imbalances over all nodes, $I_{\text{total}} = \sum_n I_n$. In this lineage, the total imbalance is, $I_{\text{total}} = 2 \times 13 + 4 + 22 + 20 = 72$, giving entropy $S_{\text{bio}} = -(2/72)\log(2/72) \times 13 - (4/72)\log(4/72) - (21/72)\log(21/72) - (22/72)\log(22/72) = 2.18$, which is rather low compared to: **(c)** One instance out of the 10^6 randomly scrambled versions of lineage 20230503-13; the number of inactive cells and their generation is the same as in the biological lineage, but their radial positions across the tree have been randomly reshuffled, hence cutting all hereditary relationships. In this tree the imbalance is more evenly distributed across the nodes than in the biological case, thus giving a much lower inheritance signal. The total imbalance is, $I_{\text{total}} = 2 \times 20 + 4 \times 5 = 60$, which gives entropy $S_{\text{scrambled}} = -(2/60)\log(2/60) \times 20 - (4/60)\log(4/60) \times 5 = 3.17$, significantly larger than the biological one. The typical entropy of the scrambled ensemble of this colony is $S_{\text{scrambled}} = 3.2$, and the largest majority of the scrambled trees have $S_{\text{scrambled}} > 2.6$ (see Fig.5), therefore making 20230503-13 a lineage where the evidence of inheritance is extremely significant (P-value $= 7 \times 10^{-6}$).

Figure S5

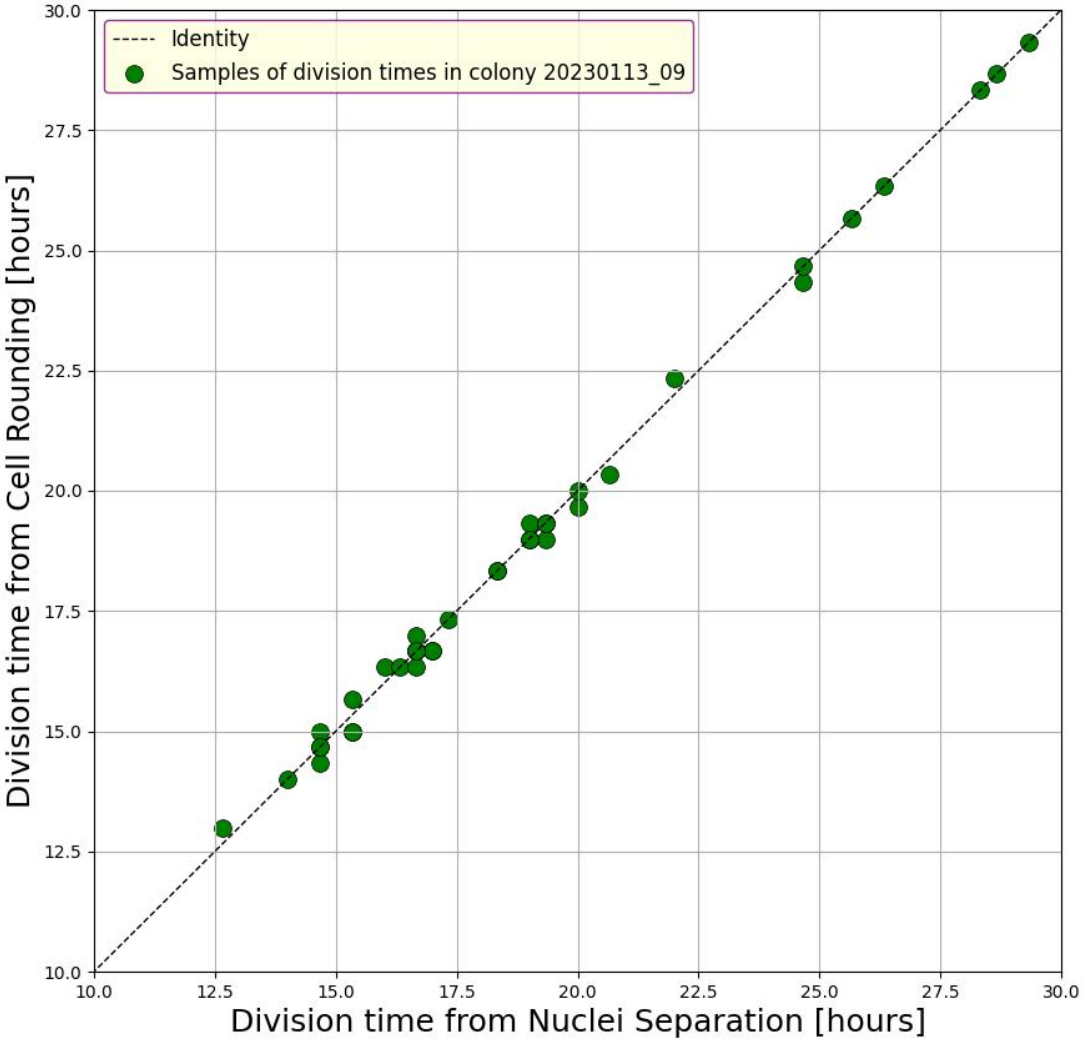

Fig S5. Different ways to determine the division times. We determine the division time, i.e. the duration of the cell cycle, through the mitotic cell rounding, a very short phase during which the cell assumes an almost spherical shape, appearing as a bright, circular object. This trait is easily recognisable in the image, which is why we use it an unambiguous time stamp of the cell cycle. An alternative time stamp of mitosis is the first image at which the two daughters' nuclei are clearly separated from each other; this criterion, however, has a larger degree of arbitrariness and it is operator-dependent, because the exact time when the two nuclei become clearly separated depends on the morphology of those particular cells. In this figure we show that these two times are anyway perfectly correlated to each other. In colony 20230113-09 we use both determinations of the division time in a subsample of mitotic events and show that the two definitions are completely equivalent.